Journal of Energy Chemistry 26 (2017) 1050–1066

Contents lists available at ScienceDirect

Journal of Energy Chemistry

journal homepage: www.elsevier.com/locate/jechem

http://www.journals.elsevier.com/journal-of-energy-chemistry/

Review

Rational design of Cu-based electrocatalysts for electrochemical reduction of carbon dioxide

Baohua Zhang, Jintao Zhang*

Key Laboratory for Colloid and Interface Chemistry of State Education Ministry, School of Chemistry and Chemical Engineering, Shandong University, Jinan 250100, Shandong, China

ARTICLE INFO

Article history:
Received 28 August 2017
Revised 8 October 2017
Accepted 10 October 2017
Available online 14 October 2017

Keywords:
Electrocatalysts
Copper
Alloy
Selectivity
CO_2 electrochemical reduction
Electrocatalytic activity
Faradaic efficiency

ABSTRACT

The recent development of Cu-based electrocatalysts for electrochemical reduction of carbon dioxide (CO_2) has attracted much attention due to their unique activity and selectivity compared to other metal catalysts. Particularly, Cu is the unique electrocatalyst for CO_2 electrochemical reduction with high selectivity to generate a variety of hydrocarbons. In this review, we mainly summarize the recent advances on the rational design of Cu nanostructures, the composition regulation of Cu-based alloys, and the exploitation of advanced supports for improving the catalytic activity and selectivity toward electrochemical reduction of CO_2. The special focus is to demonstrate how to enhance the activity and selectivity of Cu-based electrocatalyst for CO_2 reduction. The perspectives and challenges for the development of Cu-based electrocatalysts are also addressed. We hope this review can provide timely and valuable insights into the design of advanced electrocatalytic materials for CO_2 electrochemical reduction.

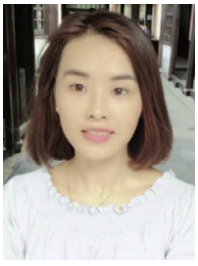

Baohua Zhang is currently a Ph.D. candidate under Prof. Zhang's supervision at Shandong University, China. She received her B.E. degree from University of Jinan in 2013. Her research interests focus on the design of advanced catalysts for electrochemical reduction of CO_2.

Jintao Zhang obtained his Ph.D. from the Department of Chemical & Biomolecular Engineering at University of Singapore in 2012. Prior to joining Shandong University as a full professor, he has been a postdoctoral fellow at Nanyang Technological University and Case Western Reserve University. His research interests include the rational design & synthesis of advanced materials for electrocatalysis, energy storage and conversion (e.g., electrocatalytic carbon dioxide reduction, water splitting, metal–air batteries, supercapacitors, and fuel cells). He has published over 40 peer-reviewed journal papers and is the author of three book chapters. These publications have earned him more than 3700 citations.

1. Introduction

At present, fossil fuels are the main energy source (over 80%) to sustain our society and economy [1]. As a result, the excess emission of carbon dioxide (CO_2) leads to the climate change and serious environmental issues [2,3]. The conversion of CO_2 to useful chemicals or liquid fuels as the renewable energy resources is a highly promising approach to addressing the forthcoming energy crisis and environmental issues [4]. Due to the sluggish reaction kinetics of carbon dioxide reduction (CDR), various approaches (such as photochemical, thermochemical, and electrochemical method) are developing to reduce the energy barrier and improve the activity, selectivity for achieving the sustainable carbon recycling [5]. Electrochemical reduction of CO_2 with the help of a proper electrocatalyst is attracting increasing attention due to its unique features. Unlike the other catalysis methods in which harsh conditions (e.g., high pressure and high temperature) needed to initiate the reaction, the electrochemical reduction reaction not only can proceed in ambient temperature and pressure, but also can generate the targeted products by reasonably adjusting the electrocatalyst, operating potential, electrolyte, and others [6,7]. Therefore, it is an important technology option for the conversion of electricity to chemical energy sources, offering the potential to create organic fuels when combined with renewable energy such as solar or wind power as shown in Fig. 1(a). Considering the sluggish reaction kinetics of the liner CO_2 molecule with a large activation energy barrier, robust and efficient electrocatalysts are

* Corresponding author.
E-mail address: jtzhang@sdu.edu.cn (J. Zhang).

https://doi.org/10.1016/j.jechem.2017.10.011

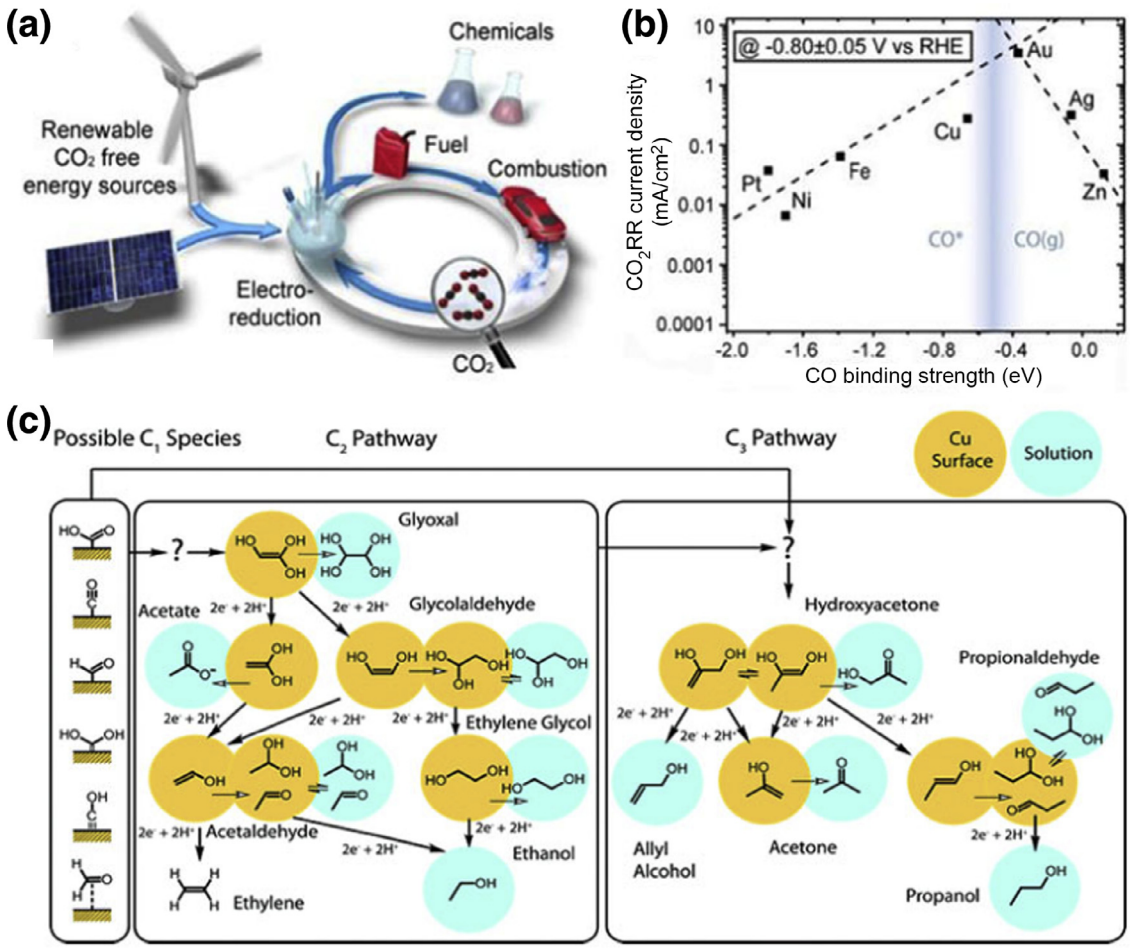

Fig. 1. (a) Electrochemical reduction of CO_2 coupled with renewable energy sources, such as solar or wind power, enables a sustainable energy cycle in which CO_2 is converted to industrial chemicals and fuels in a renewable and sustainable manner. (b) Volcano plot of partial current density for CO_2 electrochemical reduction at −0.8 V vs. CO binding strength on various metals. Reproduced with permission from Ref. [10]. (c) Proposed reaction pathways for different products on Cu electrocatalysts. Reproduced with permission from Ref. [36].

required to improve conversion efficiency of CO_2 reduction reaction [8]. However, the extensively development of this technology suffers from the high cost, low efficiency, and poor selectivity of the electrocatalysts [9,10]. Specifically, the high price of the noble metal materials hampers their extensive applications. Furthermore, the hydrogen evolution reaction as a competitive reaction often results in the poor selectivity for CDR. To resolve these tricky issues and improve the activity and selectivity of electrocatalysts for CDR, much efforts have been devoted to exploit non-noble metal electrocatalysts on the basis of nanostructure [11,12], alloying [13,14], surface modification [15,16] and so on.

In a CO_2 saturated aqueous solution, the typical CO_2 electrochemical reduction generally involves three elementary steps: first, the chemical adsorption of CO_2 molecules on an electrocatalyst surface; second, the broken of C–O bonds to form C–H bonds along with the electron transfer and/or the proton migration; finally, the rearrangement and desorption of products from the electrocatalyst surface [17,18]. As a typical example, the electrochemical reduction of CO_2 to CO is proposed according to the following process, given in Eqs. (1)–(4) [19,20]:

$$CO_2\ (g) + {}^* \rightarrow {}^*CO_2\ (ads) \quad (1)$$

$$CO_2\ (ads) + H^+\ (aq) + e^- \rightarrow {}^*COOH \quad (2)$$

$${}^*COOH + H^+\ (aq) + e^- \rightarrow {}^*CO + H_2O(l) \quad (3)$$

$${}^*CO \rightarrow CO\ (g) + {}^* \quad (4)$$

where asterisk (*) indicates a catalytic site for adsorbing a surface-bound species. CO_2 electrochemical reduction is a multistep reaction process including two-, four-, six-, or eight-electron reaction processes [21]. A series of products including CO and hydrocarbons (e.g., formic acid, methanol, ethanol, methane, aldehyde, ethylene, ethane) would be synthesized on the basis of the different reaction pathways (reactions (5)–(10)) [22,23]. The generated products such as ethanol and methanol can be directly used as fuels, usually being used to partly replacement gasoline for internal combustion engines [24]. Carbon monoxide can be converted into valuable liquid fuels or other useful chemicals through further Fischer–Tropsch process [25]. In addition, methane is main component of natural gas and ethylene can be used to produce plastics. A wide range of valuable reduced carbon compounds further concretely illustrates the significance of CO_2 electrochemical reduction.

$$CO_2 + 2H^+ + 2e^- \rightarrow CO + H_2O\ E^0 = -0.52\ V \quad (5)$$

$$CO_2 + 2H^+ + 2e^- \rightarrow HCOOH\ E^0 = -0.61\ V \quad (6)$$

$$CO_2 + 4H^+ + 4e^- \rightarrow HCHO + H_2O\ E^0 = -0.51\ V \quad (7)$$

$$CO_2 + 8H^+ + 8e^- \rightarrow CH_4 + 2H_2O \; E^0 = -0.24\,V \quad (8)$$

$$2CO_2 + 12H^+ + 12e^- \rightarrow C_2H_4 + 4H_2O \; E^0 = -0.34\,V \quad (9)$$

$$CO_2 + 6H^+ + 6e^- \rightarrow CH_3OH + H_2O \; E^0 = -0.38\,V \quad (10)$$

Carbon monoxide (CO) is an important intermediate product for CDR because CO can be further reduced to hydrocarbons and/or oxygenates electrochemically [26–28]. Thus, the binding strength of CO on various metal surfaces (Fig. 1(b)) is often used to deduce the catalytic selectivity of an electrocatalyst. Accordingly, the metal catalysts can be divided into three main groups: (1) the metals such as Au, Ag and Zn possess weak adsorption capacity for CO. Once CO is adsorbed on the surface of such a metal, the CO adsorbed (CO_{ads}) tends to be directly break away from the electrode surface, leading to a high selectivity for synthesizing CO [29]. (2) The metals including Pt, Fe and Ni with low hydrogen evolution potentials are easily covered by CO due to the strong binding ability of CO on their surfaces, leading to high selectivity for hydrogen evolution reaction (HER) [30,31]. The third type of metals (e.g., Cu) possesses intermediate binding energy for CO, which not only provides successive electron/proton transfers but also offers the potential to form C–C coupling. CO_{ads} would continue to form hydrocarbons via the subsequent hydrogenation reaction [29,32].

Therefore, among the metal catalysts for CDR, metallic Cu is the most widely studied catalysts. Hori, in a pioneering work, pointed out that Cu has the unique selectivity for CDR to generate a variety of hydrocarbons (e.g., CH_3OH, CH_3CH_2OH, CH_4, HCHO, CH_2CH_2) [32]. Therefore, much research attention has been invested to investigate the unique activity of Cu for CDR [33]. However, CO_2 reduction at a Cu electrode often requires large overpotential of more than 1 V, especially at the polycrystalline Cu electrode [32,34]. In addition, the stability of Cu is not ideal for a long time scale. As shown in Fig. 1(c), CO_2 electrochemical reduction with a cupper electrocatalyst is extremely complicated, thus, the selectivity for a targeted product cannot be controlled easily [35,36]. To address these issues, experimental and theoretical investigations have targeted to better understand these mechanisms for further improving the activity and selectivity of Cu-based catalyst [29,33,36–40]. With rapid advances on the development of Cu electrocatalysts [13,16] for CDR with a lower overpotential and better product control, it is urgent to update the recent achievements for improving the electrocatalytic activities. Herein, we summarize the recent advances for designing advanced copper-based CDR electrocatalysts. With the brief introduction on the basic principles for evaluating the catalytic activities of an electrocatalysts, the Cu-based electrocatalysts for CDR have been summarized. The challenges and future directions for developing efficient CDR electrocatalysts are also addressed.

2. Fundamental parameters for CO_2 electrochemical reduction

2.1. Onset potential, overpotential, and Tafel slope

The onset potential refers to the potential applied on an electrocatalyst vs. the reference electrode, on which a desired product is yielded at a detectable amount scale. Typically, the transition join point between the thermodynamic controlled region and the kinetic controlled region is defined as the onset potential [41]. It is worth noting that the onset potential is generally lower than the equilibrium potential for CDR. The overpotential (η) is defined as the potential difference between the standard electrode potential (E^θ) and the minimal potential applied (E) for reducing CO_2 to a specific product [42], specifically, $\eta = E^\theta - E$. The overpotential as an important index plays a crucial role in evaluating the catalytic performance of an electrocatalyst [41].

Tafel slope is another important parameter to evaluate the performance of electrocatalysts. In the case of CDR, the reduction process is farther from the equilibrium state ($\eta >> 0$). According to the Butler–Volmer equation, Tafel plot, which links the overpotential and the current density in the form of logarithm can be simply expressed as Eq. (11) [43]:

$$\eta = \left(\frac{-2.3RT}{\alpha nF}\log j^0\right) + \left(\frac{2.3RT}{\alpha nF}\log j\right) = a + b\log j \quad (11)$$

in which the exchange current density (j^0) is the common absolute value of current density at the equilibrium of the system ($\eta = 0$). α is the transfer coefficient. n is the number of electrons transferred. F is the Faraday constant. R is gas constant. T is the temperature. Tafel slope (b) is commonly used to investigate the reaction mechanism via determining the rate-determining step [44]. It is well-known that carbon dioxide reduction is an extremely complex process with multi-step and multi-electron transfer. Thus, Tafel slope would be analyzed case by case on the basis of the specific products. For the case of carbon monoxide as the dominate product (Fig. 2(a) and (b)), if the Tafel slope is close to 118 mV dec^{-1}, it implies that the rate determining step for CO_2 reduction occurs the generation of carbon dioxide radical ($CO_2^{\bullet-}$) as the key intermediate by the initial one electron transfer step (Fig. 2(a)), it is commonly invoked for metal electrodes [35]. While the Tafel slope is about 59 mV dec^{-1}, the proposed mechanism includes a fast pre-equilibrium involving one electron transfer to form $CO_2^{\bullet-}$ and a subsequent slower chemical reaction as the rate-determining step (Fig. 2(b)) [35,41,45,46].

2.2. Electrochemically active surface area (ECSA) and roughness factor (RF)

Electrochemically active surface area (ECSA) is of importance for accurately assessing the activity of an electrocatalysts, which reflect the real surface area for electrochemical reactions. Specific ways to measure ECSA of a given electrocatalyst have been summarized by Trasatti and Petrii [47], especially those of noble metal electrocatalysts, such as Pt, Pd, Au. Electrochemical determination of the charges corresponding to form a hydrogen monolayer on Pt, surface oxide monolayers for Pd and Au is often used to determine the corresponding ECSA, respectively. For the detailed ECSA measurements of Cu electrocatalysts, two approaches have been proposed, namely, the double layer capacitance differential method and the underpotential deposition (UPD) method [12,27,47,48]. For the layer capacitance differential method, the ECSA of a Cu catalyst is determined by the analysis of the double layer capacitance. Typically, the capacitive currents in a potential range without faradaic reaction are determined by cyclic voltammogram method at various scan rates, respectively (Fig. 2(c)) [49]. The specific capacitance (C_{dl} in uF) of a Cu electrocatalyst is obtained from the slope of capacitive current against scan rate (Fig. 2(d)) [49]. Then, ECSA (in cm^2) is determined by dividing the electrode capacitance with the standard double layer capacitance (C_s, 27.5 μF/cm^2 according to Eq. (12) [50]:

$$\text{ECSA} = \frac{C_{dl}}{C_s} \quad (12)$$

To demonstrate the UPD method, a typical CV curve for the UPD of Pb on a Cu electrode is shown in Fig. 2(e). The two peaks (named as C_{Ia} and C_{Ib}) at around −0.4 V before the bulk deposition of Pb (C_{II} at −0.54 V) are ascribed to the underpotential deposition of Pb on the surface of Cu. During the anodic scan, the peaks of labeled 'A_{II}' and 'A_I' are corresponding to the bulk and underpotential dissolution of Pb, respectively. On the basis of the total

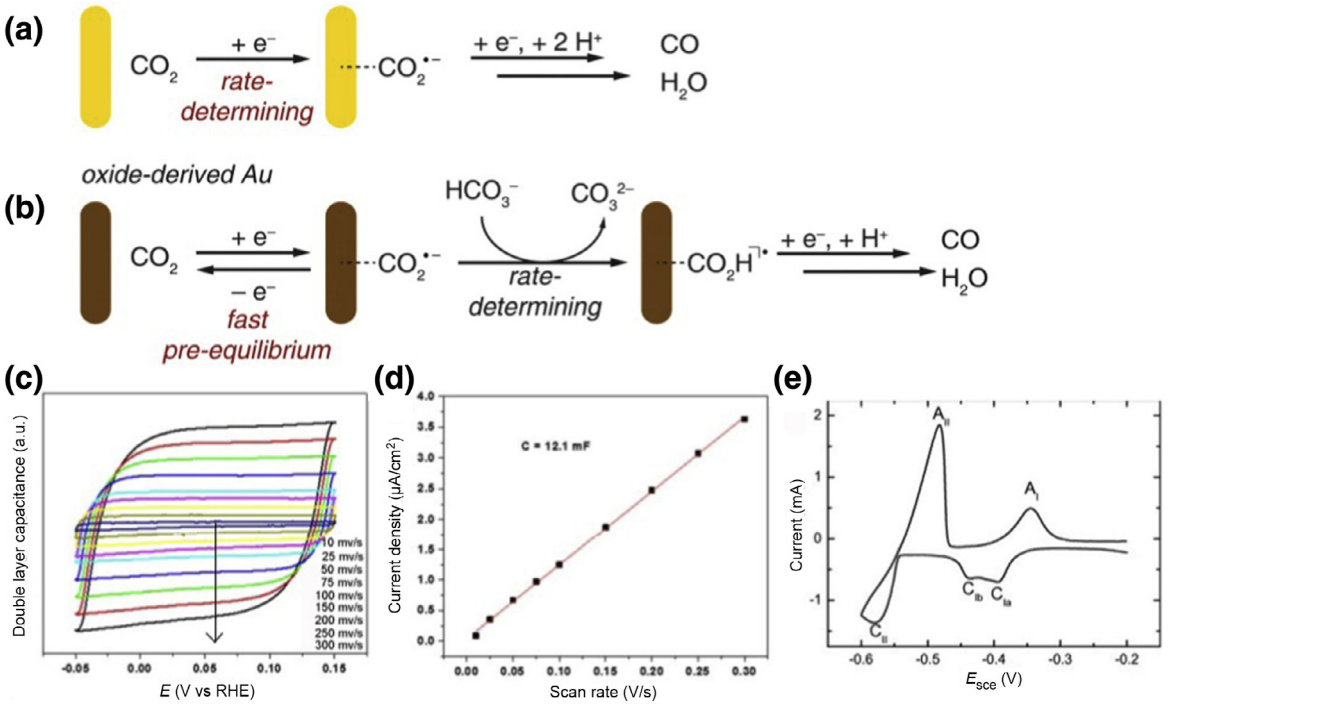

Fig. 2. (a, b) Proposed Mechanisms for CO_2 Reduction to CO. Reproduced with permission from Ref. [46]. (c) Cyclic voltammograms for a Cu substrate at various scan rates and (d) the linear relationship between the current density and scan rate. Reproduced with permission from Ref. [49]. (e) Cyclic voltammograms for a Cu substrate measured in 0.1 M $HClO_4$ + 1 mM $Pb(ClO_4)_2$. Reproduced with permission from Ref. [48].

charges for depositing a Pb monolayer during the potential range of UPD (Q_{Pb} in μC), the ECSA of Cu can be determined by dividing the conversion factor of 310 μC/cm^2 [47]. For the detailed measurements of ECSAs, the readers may be referred to the reported works [16,51,52]. The roughness factor (R_f) is actually the ratio of the electrochemically active surface area (EASA) to the geometric surface area, which is an important factor for determining the catalytic performances [20,52].

2.3. Faradaic efficiency (FE), current density and turn over frequency (TOF)

Faradaic efficiency (FE) refers to the percentage of electrons consumed for the formation of a given product. Thus, FE for a specific product is calculated using Eq. (13) [53,54]:

$$\varepsilon_{\text{Faradaic}} = \frac{\alpha n F}{j(\text{mA/cm}^2) \times t(\text{s})} = \frac{\alpha n F}{Q} \tag{13}$$

in which α is the number of electrons transferred (e.g., $\alpha = 2$ for reduction of CO_2 to CO). n refers to the number of moles for a desired product. F is Faraday's constant. Q is the charge passed (in C) for a specific reaction.

Current density is normalized to the mass or the surface area of the catalyst, which is also a crucial indicator for the reaction rate on a specific electrocatalyst. For CDR, the overall current density is often calculated via dividing the current by the geometric surface area of the working electrode. Therefore, the current density can be significantly increased by using nanostructured electrode materials with large real surface area while keeping the geometric area constant. In addition, the partial current density for a specific product can be obtained on the basis of the corresponding FE.

The turnover frequency (TOF) of a targeted product is a measurement of per-site activity of catalysts to produce the targeted product. TOF for the formation of a special product can be calculated according to Eq. (14) [55,56]:

$$\text{TOF}\ (\text{s}^{-1}) = \frac{\text{The rate of product formation}}{\text{The number of Cu surface atoms}} = \frac{i_0(\text{A cm}^{-2}) \times \text{FE}}{\text{active sites density} \times e \times n} \tag{14}$$

where active sites density (site^{-1}/cm^2) can be calculated by density of active sites for standard sample (site^{-1}/cm^2) multiplying RF. e refers to elementary charge (1.602×10^{-19} C). n refers to the number of electrons transferred to generate the special product (e.g., $n = 2$ for CO).

3. Cu-based electrocatalysts for carbon dioxide reduction

3.1. Cu nanostructures

Although Cu has been extensively studied to synthesize hydrocarbons (e.g., CH_4, C_2H_6, C_2H_4) from CO_2, electrochemical reduction of CO_2 on bulk Cu electrode generally requires a large overpotential of above 1 V, and suffers from the rapid deactivation and poor selectivity [33]. Therefore, much effort has been placed on tailoring the structures of Cu electrocatalysts in the scope of atom and/or nanoscale to improve their activities and selectivities [29,34,37]. It is found that the electrocatalytic performance of Cu catalysts is closely dependent on their particle size [57], surface structure [12], and crystal facets [58,38] and so on. To reveal the effect of surface structure on the electrocatalytic properties, different types of highly dense Cu nanowires (Fig. 3(a)) have been synthesized by thermal oxide of Cu mesh into copper oxide nanowires in air, followed by thermally forming gas reduced and electrochemical reduction, respectively. The forming gas and electrochemically reduced nanowires are denoted as FGR and ECR nanowires in the following discussion, respectively. Although the two types of nanowires exhibited the shape with similar dimension (Fig. 3(a)), they were found to possess substantially different

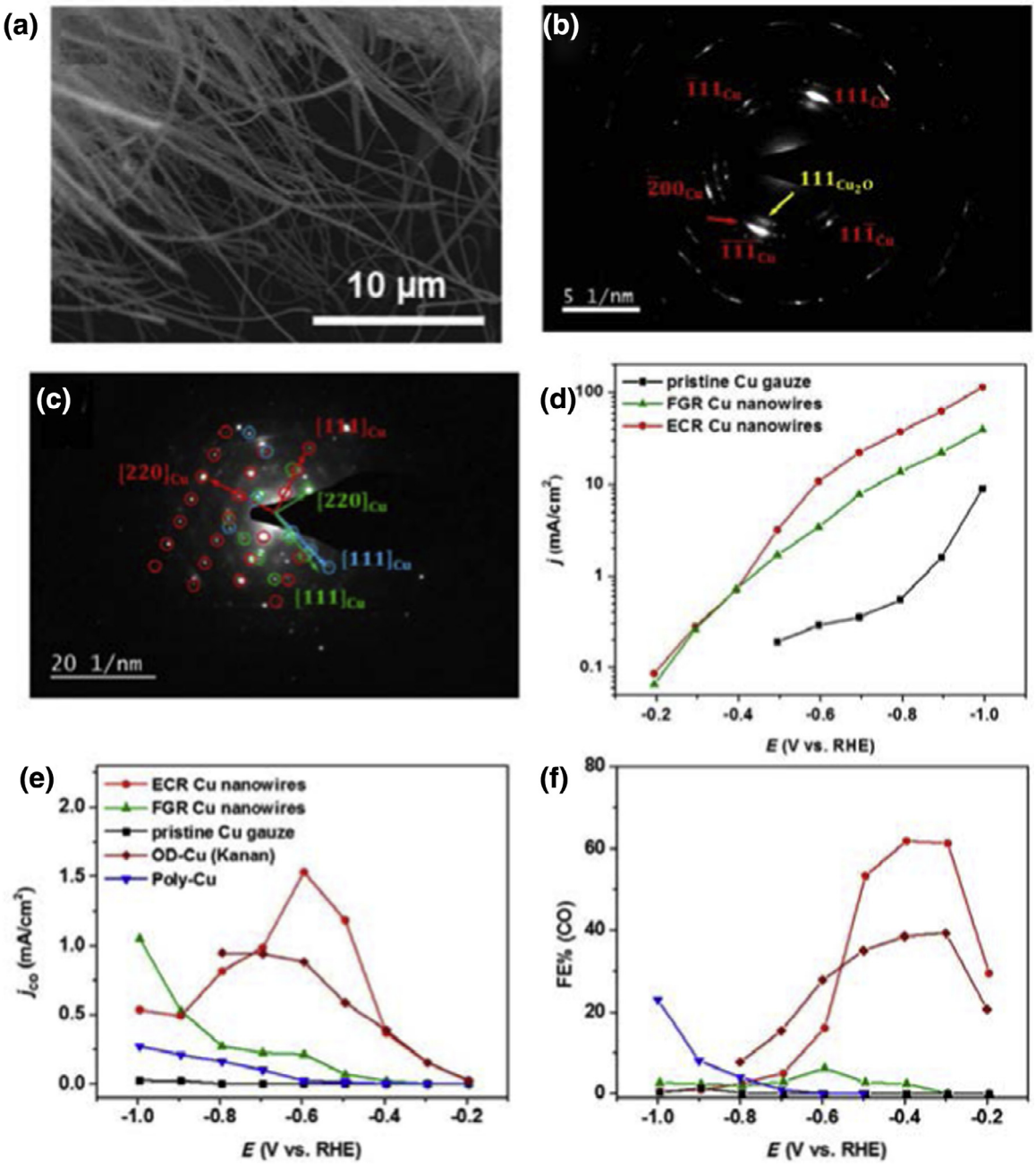

Fig. 3. (a) SEM image of Cu nanowires. (b) Selected area electron diffraction (SAED) pattern of the ECR Cu nanowires indicating the presence of both metallic Cu and Cu_2O phases (with the diffraction spots indexed in red and yellow, respectively). (c) SAED pattern of the FGR Cu nanowires showing pure metallic Cu of large crystal domains. (d) Tafel plots of the total current densities depending on the electrode potential for ECR, FGR Cu nanowires and the pristine Cu mesh. Catalytic performance of the Cu nanowires and pristine Cu gauze in comparison to oxide derived copper (OD-Cu, adapted from Ref. [12]) and polycrystalline copper (poly-Cu, adapted from Ref. [20]). (e) Partial current densities (j_{CO}) and (f) Faradaic efficiencies for CO production. Reproduced with permission from Ref. [49].

crystalline structures at the nanoscale. As shown in Fig. 3(b) and (c), selected area electron diffraction (SAED) pattern of the ECR Cu nanowires indicate the presence of both metallic Cu and Cu_2O phases. The small amount of Cu_2O is believed to be due to re-oxidation of small Cu crystalline domains on the surface when the ECR nanowires were exposed to air. However, only pure metallic Cu with large crystal domains is observed on the SAED pattern of the FGR Cu nanowires. The electrochemical results revealed that both FGR and ECR nanowires have much higher current densities for CDR compared to the pristine Cu gauze. The ECR nanowires possess the most efficient catalytic activity among the three catalysts. To reach a current density of 1 mA/cm^2, only an overpotential of 0.3 V is required (Fig. 3(d)). The current density gradually increases with increasing overpotential and reaches to the maximal value of around 1.5 mA/cm^2, which is better than the previously reported results (Fig. 3(e)) [29,36,37,59]. Notably, The FE of CO for ECR nanowires as high as ~60% can be achieved at an overpotential of only 0.3 V. ECR nanowires exhibited higher selectivity for producing CO than those of other Cu catalysts in the low-overpotential region (Fig. 3(f)). The two types of nanowires had similar dimensions. However, the ECR nanowires have higher selectivity, which can be originated from their unique surface structures. The ECR nanowires were composed of small crystalline domains in near-surface region.

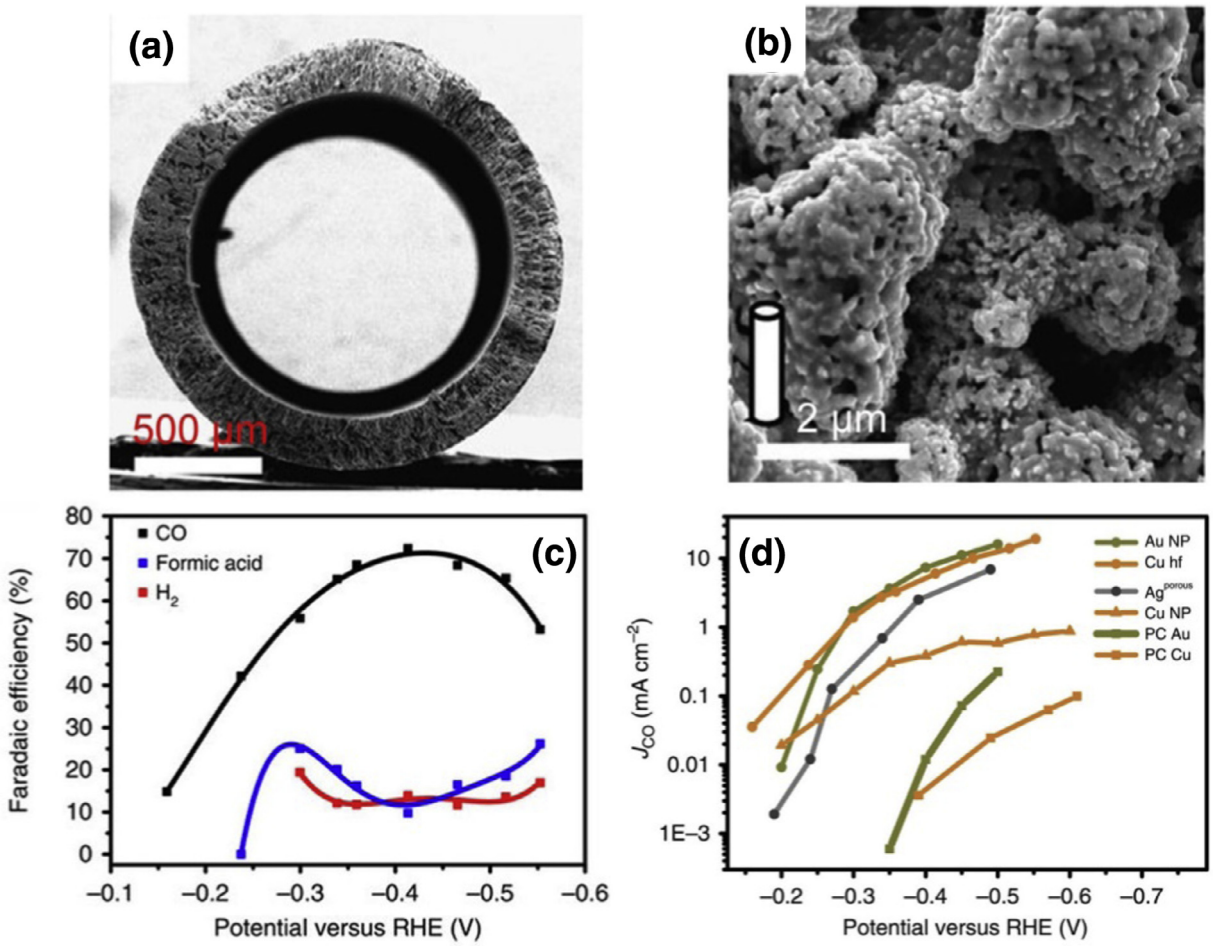

Fig. 4. (a) Cross-sectional SEM image of the Cu hollow fiber. (b) High-resolution SEM image of the outer surface of a Cu hollow fiber. (c) FE of CO, formic acid and H_2 as a function of the potentials applied. (d) Comparison of the performance of different electrodes (Au, Ag and Cu electrodes in (d) adopted from Ref. [31,62]) on the basis of the partial current density for synthesizing CO at variable potentials. Reproduced with permission from Ref. [60].

Such a nanoscale crystalline structure results in high-density grain boundaries. The grain boundaries in Cu electrodes could be many active sites for selective reduction of CO_2 to special products [28]. Additionally, the small crystalline features could also be associated with low-coordinated surface sites. According to the reported particle size effect on CO_2 reduction, the low-coordinated sites on Cu nanoparticles are believed to promote the production of CO [12].

Microtubular gas diffusion electrode (GDE) is often used for electrocatalytic reduction of CO_2 due to its unique structure for improving the reaction efficiency [61]. Recently, a novel three-dimensional porous hollow fiber copper electrode (Fig. 5(a) and (b)) has been fabricated via spinning and subsequent thermal treatment method [60]. The porous hollow fiber copper provides a large area, three-phase boundary for gas–liquid reactions. In the process of CDR, CO_2 was purged from the inside out of the fiber and gas bubbles emerge from out of the fiber. When use the synthesized Cu fiber as a catalyst for CDR, the onset of CO formation can be observed at −0.15 V (vs. RHE) (Fig. 4(c)), which is much positive than the previous reports (around −0.5 V) [29]. The sum FE for the main products reaches up to 85% at the potential range of −0.3 to −0.5 V. Especially, a maximum FE for synthesizing CO is up to ~72% at a potential of −0.4 V, much higher than those of reported polycrystalline copper [29] (only ~20% at a potential of −0.8 V) and copper nanoparticles [12] (~45% under a current density of 300 μA/ cm^2), respectively. As shown in Fig. 4(d), the electrochemical performance of such Cu hollow fibers is even comparable to the noble metal catalysts (e.g., nanoporous silver [31], gold nanoparticles [62]) at low overpotentials. In the present case, the porous hollow fiber, as an efficient gas diffuser would facilitate the rapid mass transfer for CO_2 and electrolyte to the inner active sites, thus leading to the enhanced catalytic performance.

Another efficient method to improve the catalytic activities of Cu catalysts is to fabricate Cu foams with hierarchical porosity for CDR [63,64]. This process is able to modify the catalytic surface and create more active sites. Accordingly, nanoporous Cu electrode and a variety of Cu foams with highly open porous walls have been synthesized by electrochemical deposition methods [65,66]. A template-assisted electrodeposition process was developed to prepared mesoporous Cu foams comprised of dendritic walls [64]. It is worth noting that hydrogen evolution reaction takes place at the Cu surface in the same potential range with that of Cu electrodeposition. Thus, hydrogen gas bubbles generated on the surface of Cu can be used as a geometric template for Cu electrodeposition, leading to the formation of porous Cu foam (Fig. 5(a)). As shown in Fig. 5(b), the SEM images exhibit that the walls of the porous Cu foam are composed of dendritic copper. The sizes of pores and dendritic structures increased obviously with increasing the deposition time, which would result in different catalytic activities to CDR. The mesoporous Cu foams (deposition time of 20 s) as CO_2 electrocatalysts were highly selective toward the formation of C2 products (e.g., C_2H_4 and C_2H_6) with the efficiencies of 55%. However, the formate production was significantly

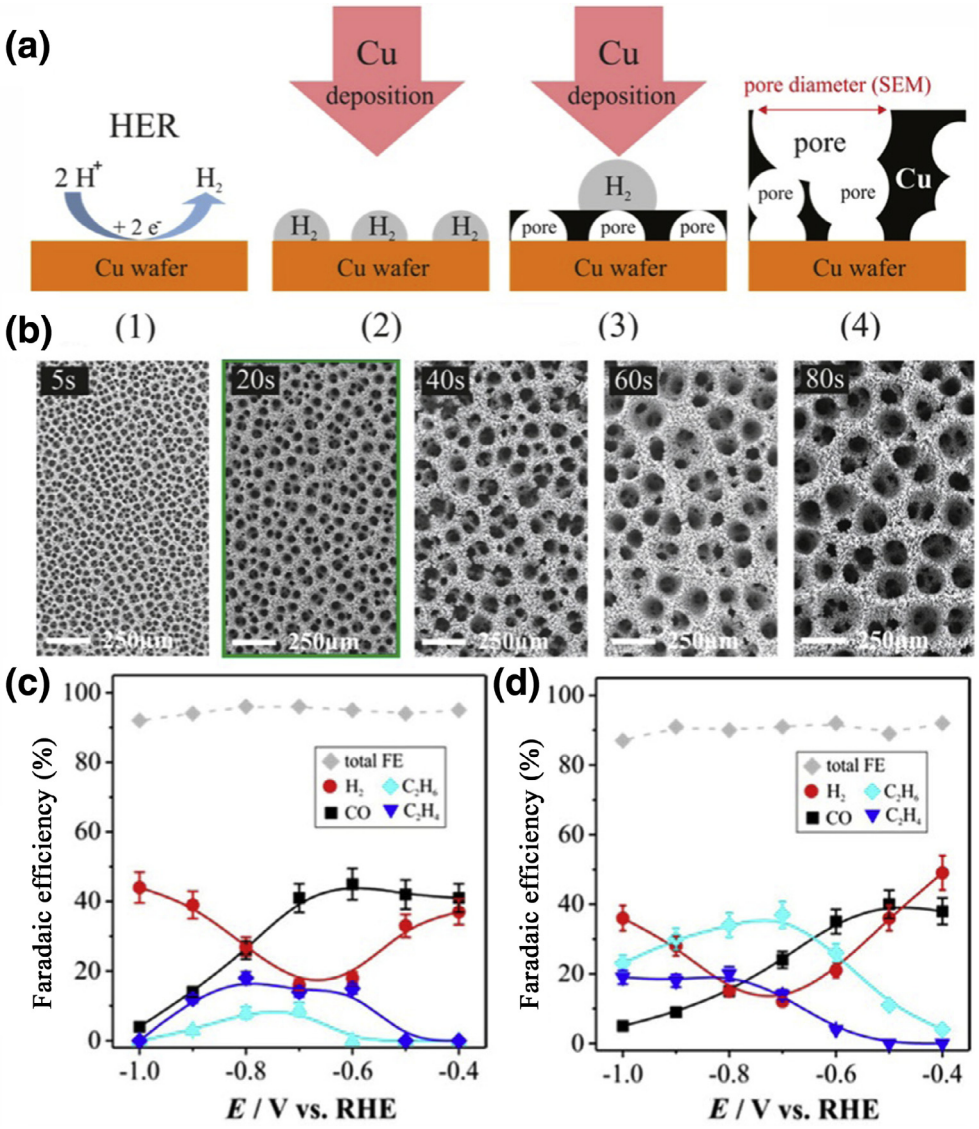

Fig. 5. (a) Schematic illustration of formation mechanism for the porous Cu foams. (b) SEM image of Cu foams synthesized at the various deposition times. Faradaic efficiencies of the CO_2 electrochemical reduction on (c) the Cu planar wafer and (d) Cu foam catalyst (deposition time of 20 s). Reproduced with permission from Ref. [64].

suppressed to very low FE efficiencies of ≤6% at the potentials applied. Generally, C_2H_4 is usually reported as the dominate C2 product for CDR [22,38,40], therefore, the extremely high production rate of the fully reduced C_2H_6 species is astonishing. Furthermore, the onset for C_2H_6 production is observed at rather low overpotentials of only −0.4 V and has better selectivity of C2 products than Cu planar wafer (Fig. 5(c) and (d)). In the present study, the observed superior C2 product efficiencies on the Cu foam can be rationalized by a combination of two particular effects. The first is related to the postdeposition treatment of the Cu foam. Cuprous oxide (Cu_2O) film formed when the Cu foam exposed to air after the electrodeposition. Therefore, the subsequent reduction of Cu_2O would create amount of active sites for C−C coupling. The second effect is that the temporal trapping of gaseous intermediates inside the mesoporous Cu foam during CDR, which is also contribute to the formation of specific C2 products.

3.2. Cu−M (M = Pd, Au, In) alloys

As discussed above, intensive research efforts have been aimed at reducing the overpotentials and improving selectivity of Cu catalysts for the CO_2 electroreduction toward a specific product, including not only experimental results (e.g., nanostructured Cu catalyst [67], oxide-derived Cu catalyst [12], core–shell structures [68–70]) but also theoretical predications (e.g., key intermediates [71], proposed reaction pathways [22,40,71]). To further improve the activity and selectivity, a series of Cu-based alloys have been synthesized [72,73].

The activity and selectivity of Cu-based catalysts for CDR are closely associated with synergistic effect. Synergistic effect is often acquired from interfacial interaction [74], geometric effects [13,53], electronic effect [13] or multicomponent system [75] and so on. Different chemical identities on the surface of the catalyst play important roles for controlling reactant adsorption, activation and product desorption. Search for the right synergistic effect is the key to develop an efficient Cu-based alloy catalyst for the electrochemical reduction of CO_2. An efficient electrocatalyst must be capable of reducing the overpotentials of CO_2 reduction and controlling the specific reaction pathways to obtain a desired product. In addition, to enhance the reaction kinetics for CO_2 reduction, the formation of Cu-based alloys is able to adjust the binding strength of intermediates on a catalyst surface, thus leading to the chemisorption and dimerization of the pertinent C1 intermediates to C2 productions [68].

To develop the bimetallic catalysts with well-defined arrangement of respective metal atoms, Ma et al. [53] synthesized a series of bimetallic CuPd catalysts with different elemental arrangements (ordered, disordered, and phase-separated, Fig. 6(a)–(c)) and different atomic ratios. The effect of structure and composition on catalyst activity and selectivity for CDR toward different products can be modulated by changing these geometric arrangements. The bimetallic CuPd alloys (Cu_{at}:Pd_{at} = 1:1) with ordered, disordered, and phase-separated atomic arrangements, were used as CDR electrocatalysts, respectively, to determine the key factors for achieving high selectivities to C1 or C2 chemicals. The ordered, disordered, and phase-separated catalysts exhibited the similar FE for CO at the relatively low potentials (> −0.3 V vs. RHE) (Fig. 6(d)–(g)). However, the C_2 chemicals start to be produced when the cathode potentials are negative than −0.3 V. Meanwhile, the ordered CuPd among the three different catalysts exhibited the highest FE of CO, and it was contrast to that of the phase-separated CuPd. The phase-separated CuPd exhibited the highest FE toward C2 chemicals up to 63%, the highest reported values for C2 production [76]. The disordered CuPd had a highest FE toward CH_4, which is in agreement with the prior reports [71]. Generally, the alloying of Cu with the other element (e.g., Pd) with a high oxygen affinity can improve the FE for CH_4. Although the ordered CuPd has more alternating CuPd sites than those of the disordered CuPd, the disordered CuPd electrode had the higher CH_4 FE may be due to the higher surface coverage of the intermediate. On the basis of the above observations, it is proposed that CO is an important intermediate for further transforming into C2 chemicals production [28,70]. Thus, by adjusting the structure of CuPd catalysts, different products of CO_2 electrochemical reduction can be obtained. For the formation of CH_4, theoretical results revealed that CO as an intermediate is easily adsorbed on the surface of Cu atoms and subsequently react with the oxygen atoms partially adsorbed on Pd atoms, leading to the generation of CH_4 [77]. However, converting CO_2 to CO or C_x productions is a relatively complex process, which can be influenced by many subtle factors [78]. Thus, improving the selectivities to different products by adjusting the geometric arrangements of bimetallic electrocatalysts should be further investigated.

Gold has been widely incorporated with Cu as bimetallic catalysts for the catalytic conversion of CO_2 into CO. As shown in Fig. 7(a), uniform AuCu bimetallic NPs with different compositions can be synthesized by the co-reduction of metal precursors as electrocatalysts for CDR [13]. The relative turnover rate (TOR) for CO at these metal nanoparticle electrodes with different atom ratios of Au/Cu (e.g., Au, AuCu, $AuCu_3$, and Au_3Cu) are shown in Fig. 7(b). It is found that the activity follows a volcano shape with a peak activity for Au_3Cu (Fig. 7(c)). The activity of Au_3Cu is around 93 times higher than that of pure Cu nanoparticles. For the conversion of CO_2 to CO, it is proposed that firstly CO_2 is adsorbed onto the surface of metal electrocatalyst to form the adsorbed intermediate (*COOH) and further reduced to CO. On the basis of the elementary steps, the TOR of CO, therefore, is highly dependent on the binding strength of adsorbed species (*COOH and CO). Previous report revealed that the optimum binding strength for *COOH and CO can be achieved on the surface of gold, leading to a peak activity for CO_2 to CO conversion according to the electronic effect. However, the best activity of Au_3Cu indicates that the presence of Cu would change the electronic structure of bimetallic catalyst, and thus the binding strength (Fig. 7(d)). Additionally, the atomic arrangement at the active site is also of importance for the efficient adsorption of intermediates according to the geometric effect. The present experimental results revealed that Au and Cu atoms are uniformly distributed following the atom ratios of their bulk compositions. Therefore, the synergic operation of electronic and geometric effects in the present case leads to the suitable binding of intermediates for the easy generation of CO rather than further reduction. The present study demonstrated that the binding strength of intermediates would be adjustable not only by changing the surface composition of bimetallic electrocatalyst according to the electronic effect, but also by correlating with the geometric effect via the local atomic arrangement at the active site. The insights gained would serve as fundamental principles for designing enhanced CO_2 electrochemical reduction catalysts.

The catalytic activity of multi-metallic nanoparticles would be enhanced by precise control on the elemental configurations down to the atomic level by the disorder-to-order transformation of individual NPs (Fig. 8(a)). Yang and co-workers exhibited that the atomic ordering transformation of AuCu NPs made them perform highly selectivity for CDR [14]. In contrast to the disordered AuCu (d-AuCu) alloy NPs, the ordered AuCu (o-AuCu) NPs is able to selectively convert CO_2 into CO at a FE of up to 80%. The formation of CO could be achieved at a low overpotential of ~200 mV. As shown in Fig. 8(b), the atomic ordered AuCu NPs can selectively enhance the production of CO. Typically, the current density for CO formation is increased from 0.43 mA/cm^2 for d-AuCu NP to 1.39 mA/cm^2 for o-AuCu NP (Fig. 8(c)). The precise control of atomic arrangements form bimetallic systems to an individual nanoparticle level provides a promising approach to adjust the catalytic properties of bimetallic catalysts and understand their structural origin. The method that regulating phase transformation between disordered alloys and ordered intermetallic in bimetallic nanomaterials has great potential to control over the level of atomic precision.

Copper–indium (CuIn) alloys due to the high selectivity for CO_2 reduction toward CO, have attracted widespread attention [79–81]. CuIn alloys through the electrochemical deposition of In on rough OD-Cu surfaces were prepared by Takanabe's group (Fig. 9(a) and (b)) [17]. The total current density and FE of CuIn catalyst at −0.3 to −0.7 V (vs. RHE) are comparable to the OD-Cu in the same potential range (Fig. 9(c)). The results indicated that there is a distinct difference in selectivity for the two catalysts. The FE of CO for CuIn catalyst are higher than OD-Cu at all applied potential. Moreover, CO is almost the sole product of CO_2 electrochemical reduction when using CuIn as catalyst, approaching a FE of 90% at −0.5 V (Fig. 9(d) and (e)). It clearly indicates that the presence of In along with Cu dramatically improves the selectivity for CO_2 reduction to CO and alters the nature of the electroactive species. In addition, the CuIn catalyst has extremely stability shown in Fig. 9(f). This preparation of non-noble metal alloy electrodes for the reduction of CO_2 provides guide lines for further improving electrocatalysis.

Porous CuIn alloy can be prepared by the reduction of $CuInO_2$ electrode, as shown in Fig. 10(a) [80]. The SEM images exhibit CuIn electrodes before and after the electrocatalytic reduction of CO_2 (Fig. 10(a) and (b)). The CuIn catalysts have superior performance over Cu electrode prepared by reducing Cu_2O for CDR (Fig. 10(c)). Fig. 10(d) indicates the product selectivities for CO_2 reduction at different potentials. During their measurement, the product distribution at an applied potential remained almost unchanged, corresponding to the highly stable nature of the CuIn electrode. It exhibits that, for the CuIn electrode, CO is formed at approximately –0.4 V and the FE for CO_2 reduction into CO and formic acid is up to 90% at –0.8 V with a low FE for H_2 of below 10%. The improved FE for CDR on CuIn electrocatalyst would be contributed to the different local electronic and/or geometric environments around the Cu sites. On one hand, the nature of the second metal (e.g., In) situated around Cu is likely to be paramount in the environment of CO_2 reduction process. On the other hand, the formation of formic acid at In electrode as a major product often occurs at high overpotentials [82–84]. Thus, the discrete nature of each component in the Cu-based system influenced the selectivity of the products from aqueous CO_2 under identical conditions. DFT calculation also indicated that In site occupation occurs on Cu step sites, and the In

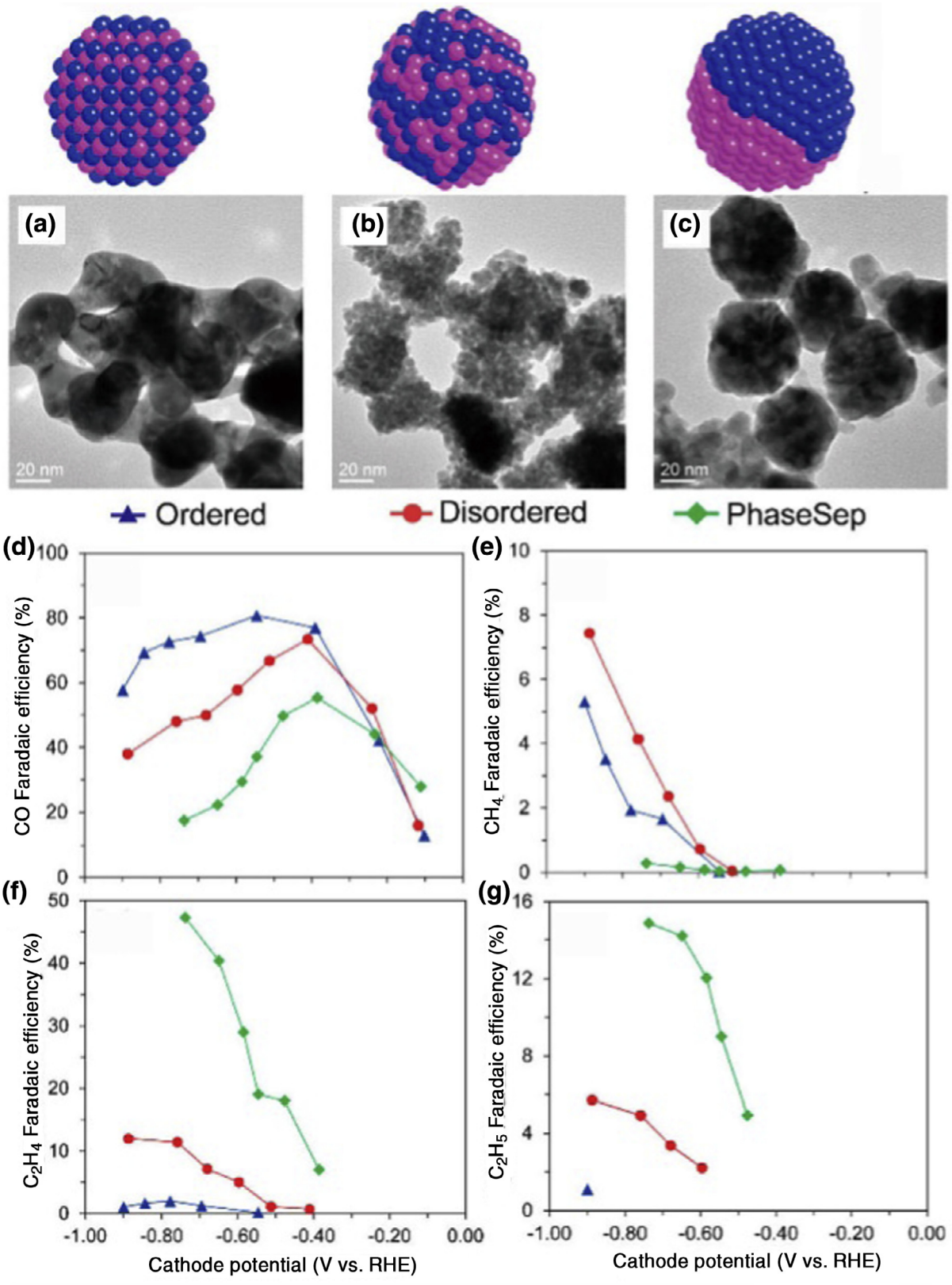

Fig. 6. Illustration and high-resolution TEM images of Cu–Pd nanoalloys with different structures: (a) ordered, (b) disordered, and (c) phase-separated. Faradaic efficiencies for (d) CO; (e) CH_4; (f) C_2H_4; (g) C_2H_5OH on bimetallic CuPd catalysts with different mixing patterns: ordered, disordered, and phase-separated. Reproduced with permission from Ref. [53].

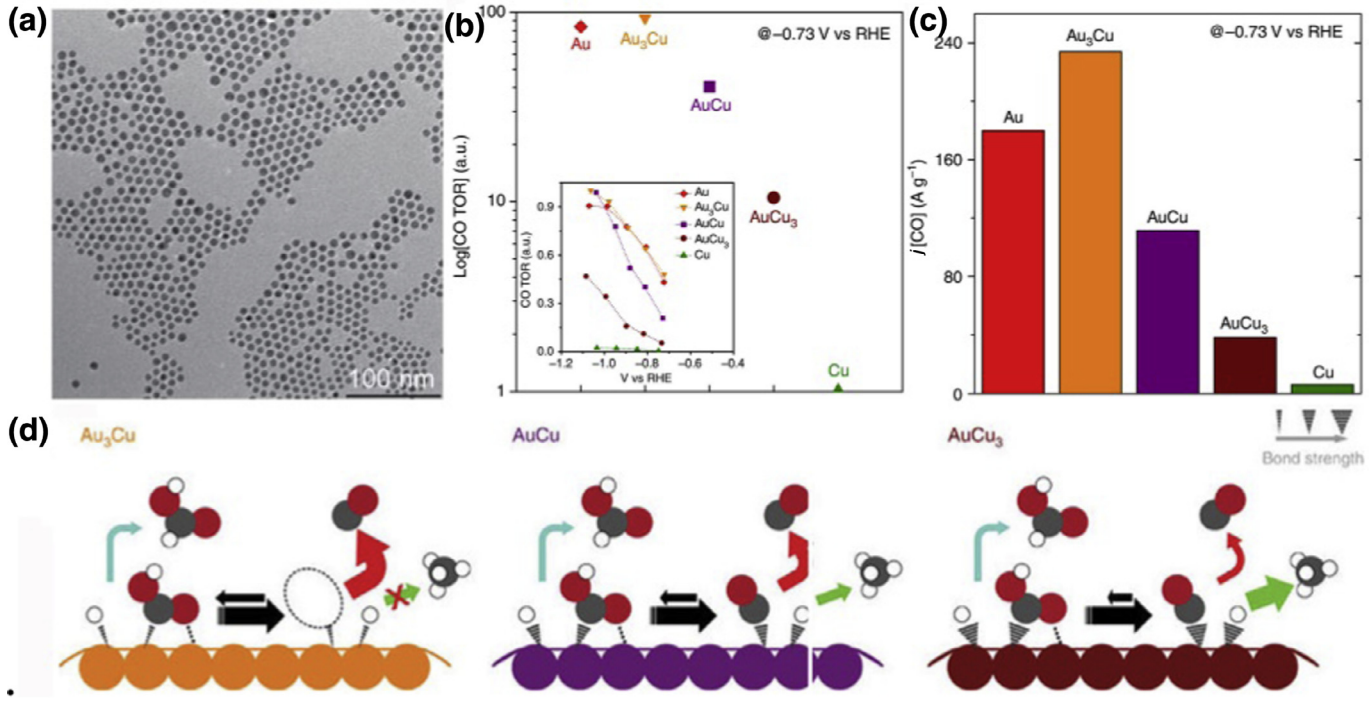

Fig. 7. (a) TEM image of AuCu nanoparticles. (b) Relative turnover rates and (c) mass activity for carbon monoxide compared at −0.73 V vs. RHE. (d) Proposed mechanism for CO_2 reduction on the catalyst surface of AuCu bimetallic NPs. The stronger the adsorption binding the thicker the wedge. C: gray, O: red, H: white. Reproduced with permission from Ref. [13].

sites hinder the adsorption of H and CO. These synergistic effects of the presence of both Cu and In account for the selectivity of electrocatalytic CO_2 reduction toward formic acid and CO. Considering the superior activity and selectivity for CO_2 reduction toward the desirable products, Cu-based alloys with various compositions and species (such as metal–metal, metal–metal oxide, metal–metal chalcogenide) are attracting attention as promising electrocatalysts.

3.3. Supported Cu electrocatalysts

To further improve the activity and selectivity of the catalysts for CO_2 reduction, great efforts have been concentrated on a more inclusive model that embraces the support materials and metal nanoparticles, this model offers new opportunities for designing and optimizing the novel catalyst systems [85]. The common support materials including reduced graphene oxide (rGO) [86], carbon nanotubes (CNTs) [15,87,88], carbon black (C black) [89], and inorganic metal oxides (MO_x) [16]) are favorable for improving the dispersion of Cu catalysts and increasing the active sites for efficient CDR. Additionally, the good electric conductivity of carbon materials and/or the strong interaction between metal nanoparticles and the supports would generate additional advantages for CDR [16,90–92]. Therefore, the species of support can influence the activity and selectivity of the catalysts. As a typical example, Bai et al. [78] revealed the support plays an important role in promoting catalytic performance because it can provide new heterogeneous sites [93], change electrical properties [94]. The synthesized ordered Pd_2Cu nanoparticles supported on different supports (SiO_2, CeO_2, Al_2O_3 and P25) for CO_2 electrochemical reduction exhibited obvious different FE and selectivity to produce CH_3OH and C_2H_5OH. Among these four catalysts, the Pd_2Cu NPs/CeO_2 showed the highest CH_3OH yield, which is probably because CeO_2 can improve Cu activity in the conversion of CO_2 to CH_3OH [95]. Pd_2Cu NPs/P25 exhibited the highest selectivity for C_2H_5OH in which the oxygen vacancies on P25 can facilitate CO_2 hydrogenation [96].

Many researches have proven that metal scattering on or into the carbon based materials is active for CDR. As a typical example, Rogers et al. [97] demonstrated that gold nanoparticles embedded in graphene nanoribbon matrix exhibited a low overpotential (onset potential > −0.2 V vs. RHE), a high Faraday efficiency (>90%), and excellent electrocatalytic stability (catalytic performance sustained >24 h) for the electrocatalytic reduction of CO_2. The catalytic environment created by the graphene nanoribbon and gold nanoparticle interaction would lead to the good catalytic performance. A carbon nanotube–gold nanohybrid as a selective and efficient electrocatalyst for CDR was prepared by a layer-by-layer method [15]. The uniform gold nanoparticles anchored on carbon nanotubes can electrocatalytic reduction of CO_2 into CO with a high selectivity at a low overpotential. Typically, a current density of 10 mA cm^{-2} for producing CO can be achieved at a low potential of −0.55 V (vs. SHE). A stable CO production rate of 0.52 mmol s^{-1} can be maintained for over 4 h, suggesting the good stability. However, the carbon-supported Cu nanoparticles have not been extensively investigated thus far due to the sensitivity of Cu to oxidation and the experimental difficulties to synthesize small size nanoparticles. But still a few studies about the carbon-supported Cu nanoparticles for CDR have been reported. As a typical example, the electrocatalytic activities of Cu nanoparticles supported on various carbon supports including carbon black (VC), single-wall carbon nanotubes (SWNTs), and Ketjen Black (KB) for CDR have been investigated [16]. The synthesized catalysts were titled as 40 wt% Cu/VC, 20 wt% Cu/SWNT, and 50 wt% Cu/KB and 20 wt% Cu/VC. Particle sizes for 40 wt% Cu/VC, 20 wt% Cu/SWNT, 50 wt% Cu/KB, and commercial 20 wt% Cu/VC catalyst (Premetek, Inc.) are summarized. Among them, the 40 wt% Cu/VC (12 nm) and the 20 wt% Cu/SWNT (19 nm) have relatively smaller size. As shown in Fig. 11(a) and (b), Cu nanoparticles are well-dispersed on VC and SWNTs. Faradaic efficiencies of two carbon-supported Cu catalysts toward CO_2 electroreduction to hydrocarbons are compared to that of electrodeposited smooth Cu films (Fig. 11(c)–(e)). For all the catalysts studied, the only hydrocarbons are CH_4 and

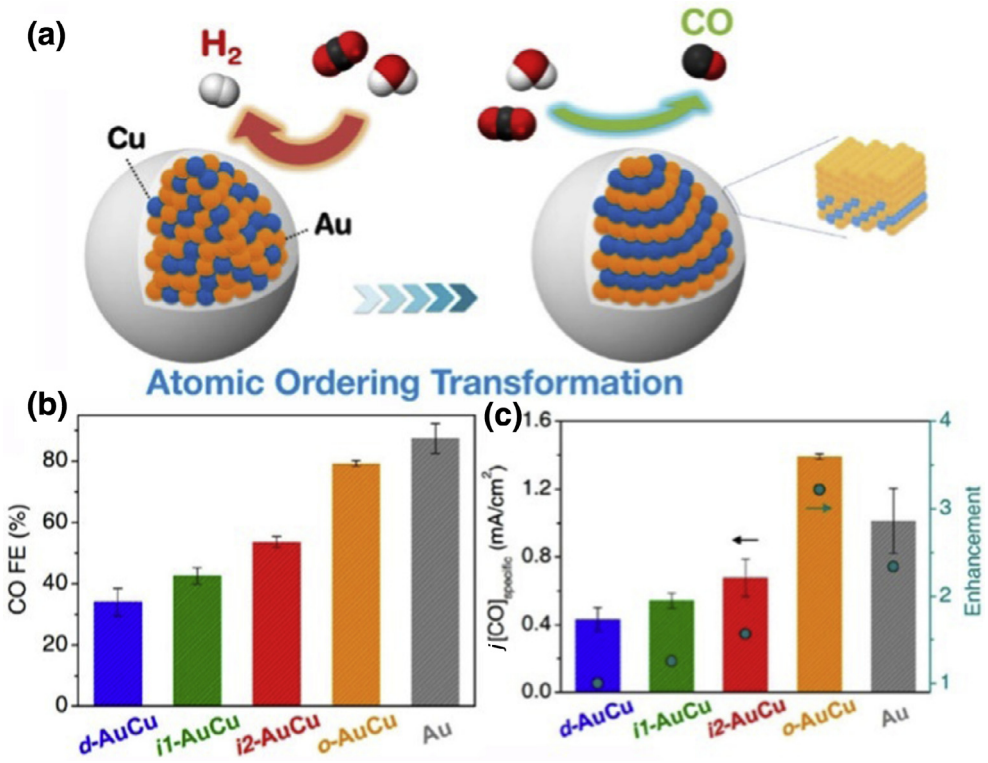

Fig. 8. (a) Illustration of ordering transformations in AuCu bimetallic NPs for CO_2 reduction. CO faradaic efficiencies (b), CO partial current density (c) at AuCu nanoparticle electrodes for electrocatalytic CO_2 reduction. Reproduced with permission from Ref. [14].

C_2H_4. For 40 wt% Cu/VC and 20 wt% Cu/SWNT catalysts, the significant onset potential positive shift (200 mV) for C_2H_4 generation in comparison with electrodeposited Cu indicates their higher activity toward C_2H_4 generation. At higher overpotentials, the CO FE decreased with the increasing FE of CH_4 and C_2H_4 due to the consumption of CO in the formation process of CH_4 and C_2H_4 [98,99]. For the supported Cu nanocatalysts, the ratio of C_2H_4/CH_4 FEs is believed to be a function of particle size, as higher ratios are observed for smaller Cu nanoparticles. This is likely due to an increase in the fraction of under-coordinated sites, such as corners, edges, and defects as the nanoparticles become smaller. The work demonstrates a new strategy to improve catalytic activity and selectivity of Cu NPs for the electrochemical reduction of CO_2 for sustainable chemistry and energy applications.

Sun and co-workers also investigated the electrocatalytic activity and selectivity of Cu NPs deposited on graphene sheets for electrochemical reduction of CO_2 into hydrocarbons [100]. Monodispersed Cu nanoparticles assembled on the pyridinic nitrogen rich graphene (p-NG) showed a mass- and size-dependent catalysis for the selectively electrochemical reduction of CO_2 to C_2H_4. The 7 nm Cu NPs assembled on the p-NG with the p-NG/Cu mass ratio of 1:1 (p-NG−Cu−7), exhibited the best electrocatalytic activity and selectivity to C_2H_4 (Fig. 12(a)). The FE for C_2H_4 formation and the hydrocarbon selectivity reached to ~19 and 79%, respectively at −0.9 V (vs. RHE) (Fig. 12(b)). To understand the effect of p-NG on the catalytic activity of composite catalyst for the CO_2 reduction, the pure p-NG as the catalyst for the CO_2 reduction was studied. It revealed that the pure p-NG yielded formate with a 65% FE and 100% hydrocarbon selectivity at 0.9 V (Fig. 12(c)). The synthesized p-NG−Cu−7 exhibited much higher selectivity for the formation of formate at −0.8 V, and C_2H_4 in the potential range of −0.9 to −1.1 V (Fig. 12(d)). These results manifest that the p-NG as a support plays a significant role in enhancing the Cu NP catalyst selectivity toward C_2H_4 at −0.9 V and more negative potentials. For the p-NG−Cu composite, the pyridinic-N of p-NG would function as active sites for anchoring CO_2 and proton, facilitating hydrogenation and carbon–carbon coupling reactions on Cu for the formation of C_2H_4. The present method demonstrates that the combination of CuNP and p-NG is an efficient way to improve the electrocatalytic activity and selectivity for CO_2 electrochemical reduction by strong interaction between the p-NG and CuNP [90–92]. The reported synthesis and assembly offers a general approach to prepare a new class of p-NG−NP catalysts for the electrochemical reduction of CO_2 with much enhanced activity and selectivity.

To reveal the effect of the interaction between compositions and carbon support of an electrocatalyst on the selectivity for efficient conversion of CO_2, PdCu and Pd with different compositions were loaded on a carbon support via thermal treatment (Fig. 13(a) and (b)). As demonstrated in Fig. 13(c) and (d), $Pd_{85}Cu_{15}/C$ catalyst shows the highest CO FE of 86% with a CO current density of 6.9 mA/cm^2 at −0.89 V (vs. RHE), which is about 5 times, 8 times higher than that of Pd/C catalyst, respectively [72]. $Pd_{85}Cu_{15}/C$ catalyst has the high selectivity of CO production due to the optimal atom ratio between Cu and Pd and the presence of low-coordination active sites. This study demonstrates great potentials of different composition PdCu alloy nanoparticles on the carbon support for the selective electrochemical reduction of CO_2 to CO. In short, assembling the metal on the various supports as electrocatalysts for CO_2 electrochemical reduction has great influence on improving the activity and selectivity of catalysts, especially for desired hydrocarbons products. Designing the Cu-based composites as electrocatalysts for CO_2 electrochemical reduction is a promising strategy for developing the CO_2 reduction technology.

More recently, metal-organic frameworks (MOFs) with uniformly porous structure have also been used to synthesize desired electrocatalysts for CO_2 electroreduction [101–105]. The direct carbonization of MOFs is a straightforward pathway to fabricate metal and porous carbon hybrid materials [106–107]. This

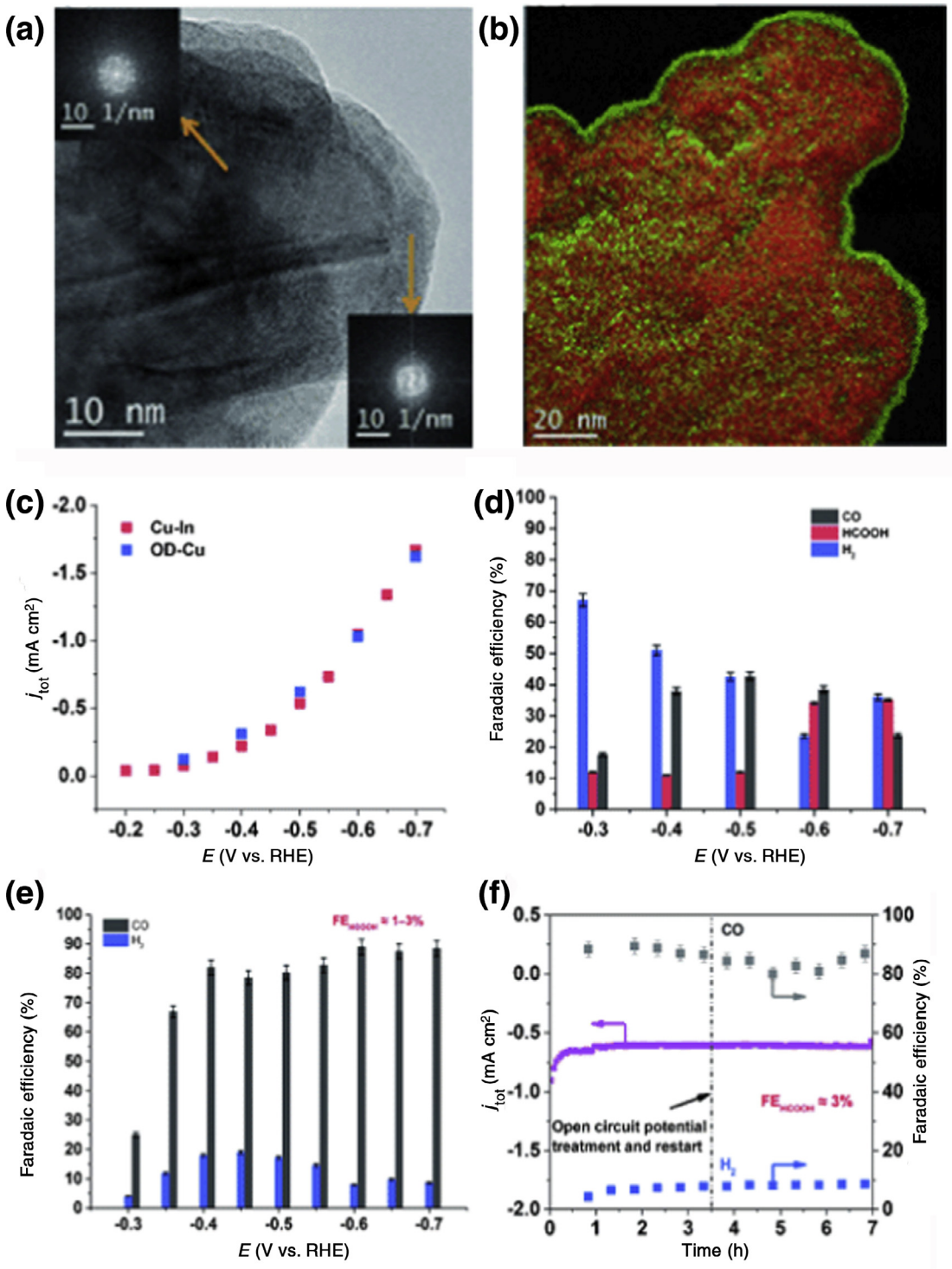

Fig. 9. (a) High-resolution transmission electron micrographs (HR-TEM) image of CuIn with Fourier transform (FFT) patterns from the bulk and the surface (inset). (b) Electronic differential system (EDS) element mapping of the selected area: In (green), Cu (red). (c) Comparison of the current density profiles for OD-Cu and CuIn. Chronoamperometric analyses of (d) OD-Cu and (e) CuIn, and (f) the long-term stability test for the CuIn catalyst at −0.6 V in 0.1 M $KHCO_3$ saturated with CO_2. Reproduced with permission from Ref. [26].

approach not only can obtain porous carbons directly from MOFs during the process of high-temperature treatment, but also incorporate the metal species of MOFs into carbon matrix in situ. Such MOF-derived composite materials exhibit many distinct merits, such as hierarchical porous structures, well-dispersed metal nanoparticles, and large surface areas, possibly benefiting to the enhanced electrocatalytic activities. For example, oxide-derived Cu/carbon (OD Cu/C) catalysts have been synthesized by a facile hydrothermal and subsequent carbonization of Cu-based MOFs [108]. The obtained catalysts prepared at various temperatures of 900, 1000, and 1100 °C are denoted as OD Cu/C-900, OD Cu/C-1000 and OD/C-1100, respectively. As shown in Fig. 14(a) and (b), the octahedral OD Cu/C composite catalysts are decorated with lots of Cu and Cu_2O particles. The OD Cu/C-1000 catalyst exhibits the

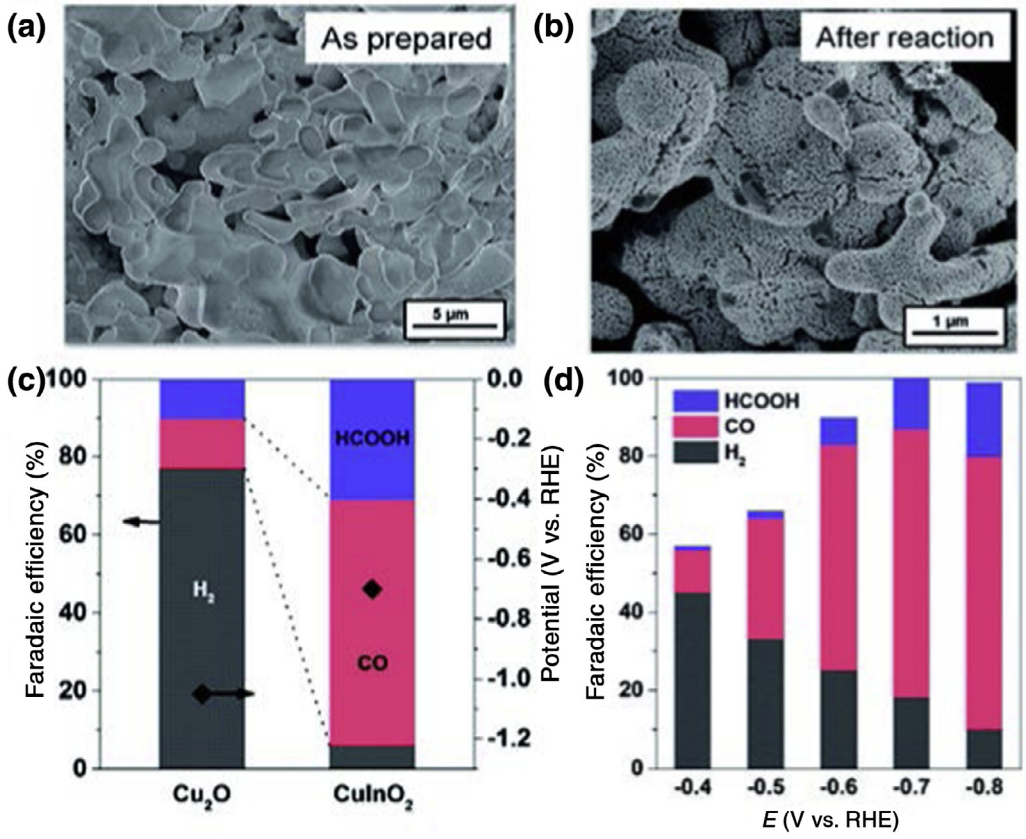

Fig. 10. SEM images of the as-prepared (a) and after-electrolysis (b) CuIn electrodes. (c) Comparison of the chronopotentiometric results of Cu-based electrodes at a j_{tot} of 1.67 mA cm^2 and (d) Faradaic efficiencies of the CuIn electrode in 0.1 M $KHCO_3$ saturated with CO_2. Reproduced with permission from Ref. [80].

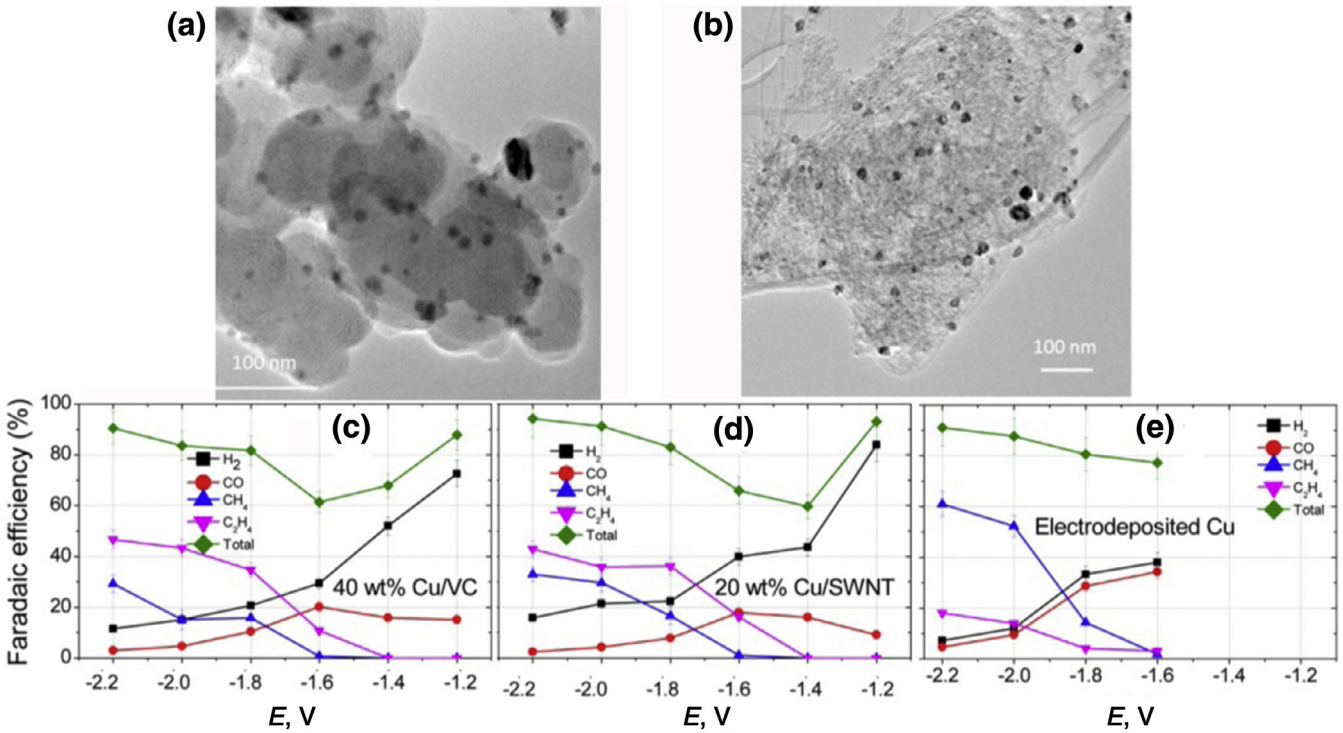

Fig. 11. TEM images of (a) 40 wt% Cu/VC and (b) 20 wt% Cu/SWNT. Faradaic efficiencies vs. potential for H_2, CO, CH_4, and (c) C_2H_4 generation at thin films of 40 wt% Cu/VC, (d) 20 wt% Cu/SWNT, and (e) electrodeposited Cu. Reproduced with permission from Ref. [16].

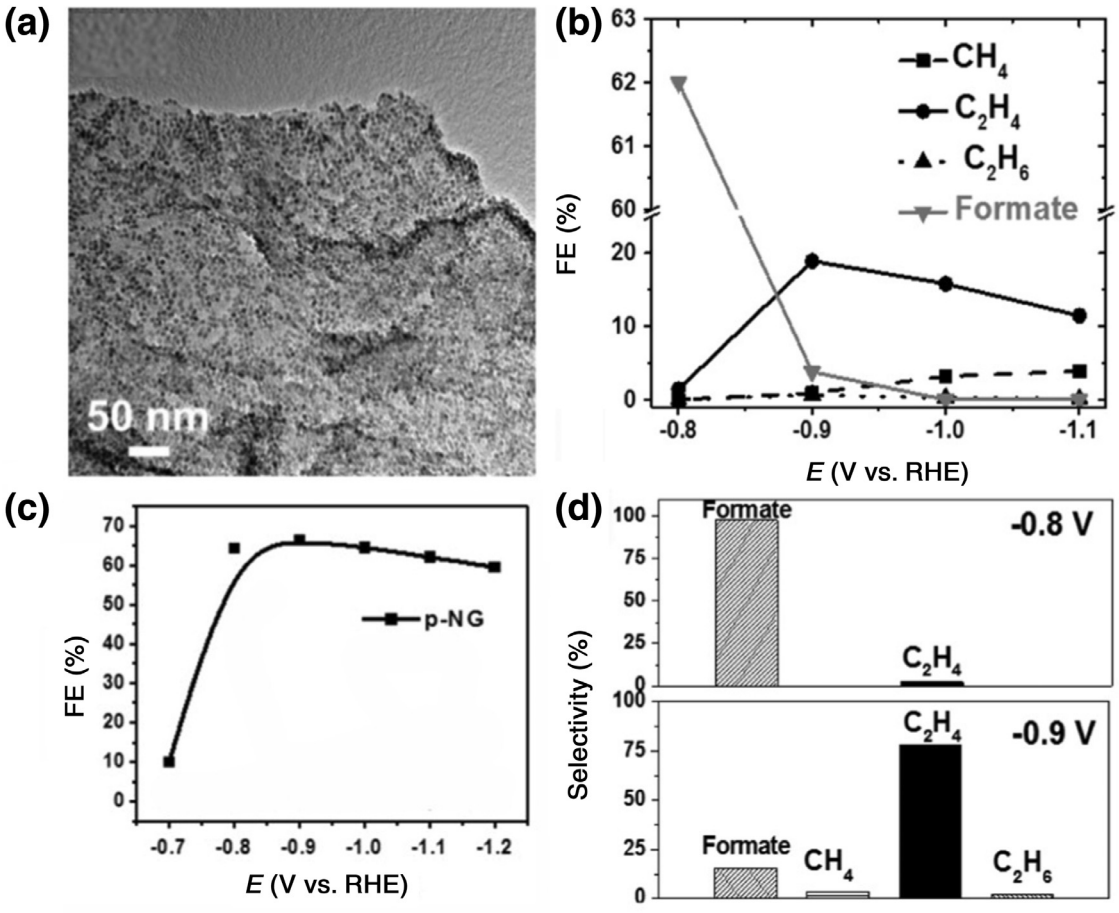

Fig. 12. (a) TEM images of p-NG–Cu–7 catalysts. (b) Reduction potential dependent FE of the p-NG–Cu–7 for CO_2 electrochemical reduction toward various hydrocarbons. (c) Product selectivity of the p-NG–Cu–7 for CO_2 reduction to hydrocarbons at −0.8 V and −0.9 V. (d) Selectivity of C_2H_4 and all other hydrocarbons generated at various potentials. Reproduced with permission from Ref. [100].

highest current density than those of OD Cu/C-900 and OD Cu/C-1100 (Fig. 14(c)) due to its lower charge transfer resistance for CDR. OD Cu/C-1000 presents high-yields of methanol and ethanol with the production rates of 5.1–12.4 and 3.7–13.4 mg L^{-1} h^{-1}, respectively (Fig. 14(d)). More importantly, the electrocatalyst exhibited the lowest overpotentials for CO_2 to C_2H_5OH. The high selectivity for the formation of ethanol would be contributed to the presence of Cu_2O in OD Cu/C because Cu_2O has been identified as an important contributor for generating alcohols at a low overpotential on oxide-derived Cu electrode [109,110] (Fig. 14(e)). Fig. 14(f) gives the possible reaction paths for CO_2 electroreduction on OD Cu/C-1000. As shown in Eqs. (1)–(3), along with one electron transfer, the subsequent formation of adsorbed intermediates (e.g., CO_2^{*-}, *COOH) would lead to the formation of formate acid and methanol via the proton-electron pair forms. In contrast, the formation of surface-bound C1 oxygenates (*CO) via the breaking of the C–O bond along with the removal of water molecule is of importance for the subsequent coupling of C–C bond to form enol-like surface species (right side). The enol-like intermediates are then converted to ethanol by hydrogenation and dehydroxylation. The improvements in activity and selectivity of the oxide-derived Cu/carbon catalysts would be contributed the synergistic effect between the highly dispersed Cu-based active species and the highly conductive carbon matrix [111,112].

4. Summary and outlook

With the rapid accumulation of CO_2 due to the burning of fossil fuels, the electrochemical conversion of CO_2 to valuable products is attracting extensive attention. However, CO_2 is a stable and inert molecule which brings significant challenges for its chemical activation to useful products. Previous efforts have been devoted to metal-based catalytic systems, especially for Cu-based catalysts. However, it is still challenging to efficiently reduce CO_2 to the targeted products. Actually, in terms of the current electrocatalytic technologies in CDR area, there is still a long way to reach the requirements for practical applications. The scientific problems mainly include high overpotential, inferior selectivity, low activity, and unsatisfactory catalyst stability. In view of the former research on the Cu-based catalysts devoted to CO_2 electrochemical reduction, we summarize the recent major advances on the development of Cu-based electrocatalysts, with special focus on the design of Cu nanostructures, Cu-based alloys, and supported Cu electrocatalysts for enhancing the activity and selectivity to CO_2 electrochemical reduction:

(1) Nanostructured Cu catalysts for carbon dioxide reduction.

The structure of electrocatalyst plays an important in boosting the final catalytic performance, especially for metal catalysts. Therefore, the preparation of nanostructured Cu catalysts is efficient to improve the current densities in comparison with the bulk material catalysts due to the larger electrochemical active surface. What's more, the rough surfaces and small crystalline features of Cu nanostructures possess significantly more low-coordination active sites (such as edges, steps, defects) than those of smooth ones, which have better intrinsic reaction activity and selectivity for CO_2 reduction to special products. In additions, the surface morphology effect, exposed crystal face and surface impurities should also

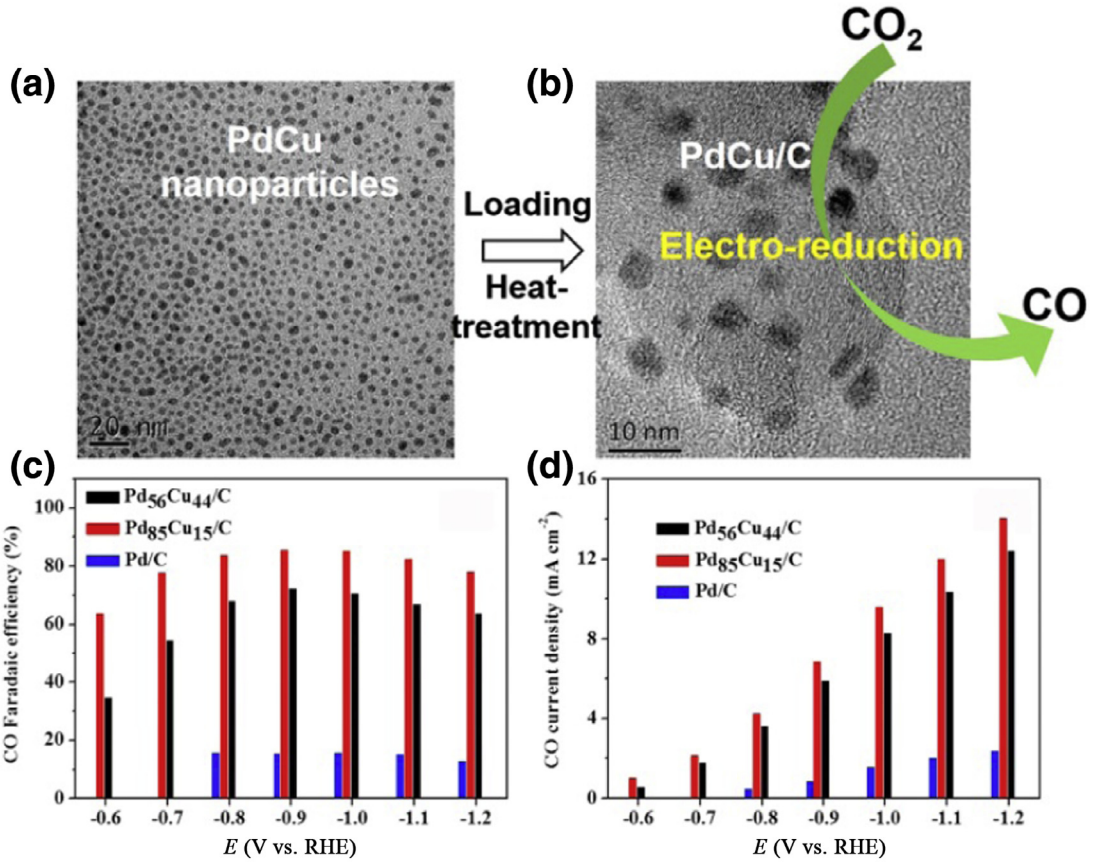

Fig. 13. TEM images of (a) the bimetallic $Pd_{85}Cu_{15}$ nanoparticles and (b) $Pd_{85}Cu_{15}$/C. CO_2 reduction activity over PdCu/C and Pd/C catalysts. (c) FE of CO. (d) Current density for CO production. Reproduced with permission from Ref. [72].

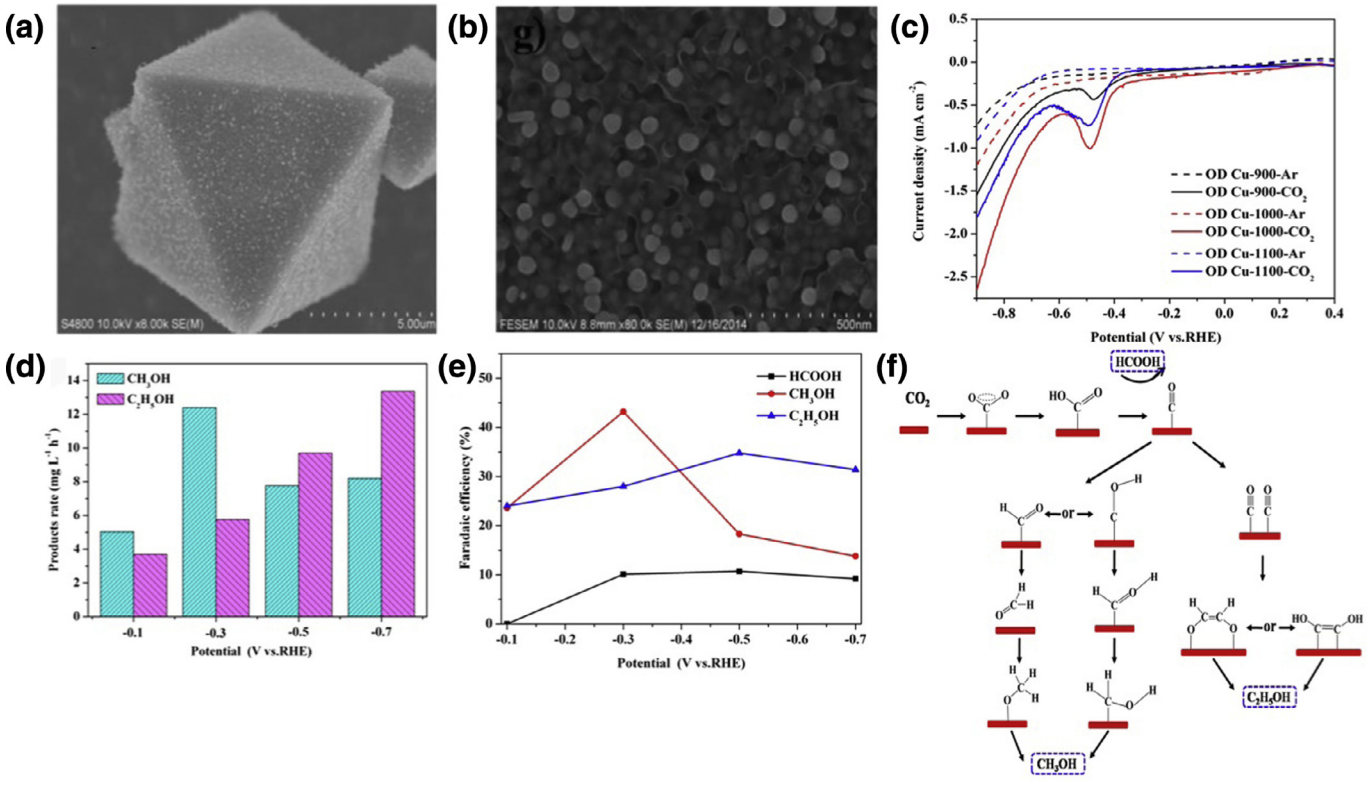

Fig. 14. (a, b) SEM images of the OD Cu/C-1000. (c) Linear sweep voltammetry curves of OD Cu/C materials in Ar- or CO_2-saturated solution with a scan rate of 50 mV s^{-1}. (d) Methanol and ethanol production rates of OD Cu/C-1000 for CO_2 electrochemical reduction. (e) Faradaic efficiency of OD Cu/C-1000 for CO_2 electrochemical reduction. (f) Proposed reaction paths for CO_2 electroreduction on OD Cu/C-1000, producing HCOOH, CH_3OH, and C_2H_5OH. Reproduced with permission from Ref. [108].

be considered. For the sustainable development of the technology in CO_2 reduction, various nanostructured Cu materials (e.g., mesoporous structures, nanowires, core–shell structures, hollow structures, multidimensional structure, metal–organic frameworks) would be further designed as promising electrocatalysts for CO_2 reduction.

(2) Composition modification of Cu for carbon dioxide reduction.

Composition of the electrocatalysts also has a significant impact on the final catalytic performance. Especially, the Cu-based alloys catalysts often have higher catalytic activities than monometallic catalysts. The bimetallic composition modification approach would alter the geometric environment and the local electronic structure, therefore the binding strengths of different reaction intermediates to Cu alloy catalysts would be adjusted properly, leading to better catalytic performance than those of monometallic catalysts. DFT calculations would provide efficient predications for designing Cu-based bimetallic electrocatalysts by changing the conventional electronic structure, and/or geometric and ensemble effects of the metal active sites. Therefore, it is still popular to rationally design Cu-based alloy catalysts with adjustable composition and desirable structure, aimed to improve the catalytic activity and selectivity for CO_2 toward desirable products.

(3) Design of Cu with catalyst support for carbon dioxide reduction

To further improve the activity and selectivity of the catalysts for CO_2 reduction, the support materials combined with Cu nanoparticles offer new opportunities for designing and optimizing the novel catalyst systems. The common support materials (e.g., rGO, CNTs, C black, or MO_x) at the nanometer scale are favorable for increasing the amount of active catalyst area per unit of electrode and improving the dispersion of the catalyst. In addition, the strong interaction between the supports and Cu nanoparticles are attractive for tuning the electronic microenvironment of the catalysts with an important influence on the selectivity for CO_2 electrochemical reduction. In short, the incorporation of Cu with desirable supports as efficient electrocatalysts for CO_2 electrochemical reduction is a promising strategy for developing the CO_2 reduction technology.

The preparation of catalysts with high activity and selectivity toward the special product would be the dominant future trends for electrochemical CO_2 reduction. The electrocatalytic activity and the selectivity of the electrocatalysts for CO_2 electrochemical reduction largely depends on the binding strength of various reaction intermediates to electrocatalysts. Therefore, the deep understanding on the reaction mechanisms on the basis of the experimental results and theoretical calculations would provide useful principles for the rational design of efficient catalysts. This review article hopes to stimulate future research interest in the development of efficient Cu-based electrocatalysts with new nanostructures, tunable compositions and efficient catalyst supports for CDR. The application of Cu-based catalysts for CO_2 reduction is still in its early stages, and further development of rationally designed Cu-based catalysts will be highly demanded.

Acknowledgments

This work was financially supported by the Natural Scientific Foundation of China (no. 21503116), the Open Funds of the State Key Laboratory of Organic–Inorganic Composites, Beijing University of Chemical Technology (oic-201601008) and the Qingdao Basic & Applied Research Project (15-9-1-100-jch). Taishan Scholars Program of Shandong Province (no. tsqn20161004) and the Youth 1000 Talent Program of China are also acknowledged.

References

[1] S. Buller, J. Strunk, J. Energy Chem. 25 (2016) 171–190.
[2] X.Q. Zhang, X.B. Cheng, Q. Zhang, J. Energy Chem. 25 (2016) 967–984.
[3] C. Federsel, R. Jackstell, M. Beller, Angew. Chem. Int. Ed. 49 (2010) 6254–6257.
[4] R. Passalacqua, S. Perathoner, G. Centi, J. Energy Chem. 26 (2017) 219–240.
[5] S.S. Han, Y.F. Chen, S. Abanades, Z.K. Zhang, J. Energy Chem. 26 (2017) 743–749.
[6] L.X. Zhang, S.Q. Hu, X.F. Zhu, W.S. Yang, J. Energy Chem. 26 (2017) 593–601.
[7] Y. Lum, Y. Kwon, P. Lobaccaro, L. Chen, E.L. Clark, A.T. Bell, J.W. Ager, ACS Catal. 6 (2016) 202–209.
[8] A.M. Appel, J.E. Bercaw, A.B. Bocarsly, H. Dobbek, D.L. DuBois, M. Dupuis, J.G. Ferry, E. Fujita, R. Hille, P.J. Kenis, C.A. Kerfeld, R.H. Morris, C.H. Peden, A.R. Portis, S.W. Ragsdale, T.B. Rauchfuss, J.N. Reek, L.C. Seefeldt, R.K. Thauer, G.L. Waldrop, Chem. Rev. 113 (2013) 6621–6658.
[9] C. Costentin, Chem. Soc. Rev. 42 (2013) 2423–2436.
[10] K.P. Kuhl, T. Hatsukade, E.R. Cave, D.N. Abram, J. Kibsgaard, T.F. Jaramillo, J. Am. Chem. Soc. 136 (2014) 14107–14113.
[11] D.F. Gao, F. Cai, Q.Q. Xu, G.X. Wang, X.L. Pan, X.H. Bao, J. Energy Chem. 23 (2014) 694–700.
[12] C.W. Li, M.W. Kanan, J. Am. Chem. Soc. 134 (2012) 7231–7234.
[13] D. Kim, J. Resasco, Y. Yu, A.M. Asiri, P.D. Yang, Nat. Commun. 5 (2014) 4948.
[14] D.Y. Kim, C.L. Xie, N. Becknell, Y. Yu, M. Karamad, K. Chan, E.J. Crumlin, J.K. Nørskov, P.D. Yang, J. Am. Chem. Soc. 139 (2017) 8329–8336.
[15] T.N. Huan, P. Prakash, P. Simon, G. Rousse, X. Xu, V. Artero, E. Gravel, E. Doris, M. Fontecave, ChemSusChem 9 (2016) 2317–2320.
[16] O.A. Baturina, Q. Lu, M.A. Padilla, L. Xin, W.Z. Li, A. Serov, K. Artyushkova, P. Atanassov, F. Xu, A. Epshteyn, T. Brintlinger, M. Schuette, G.E. Collins, ACS Catal. 4 (2014) 3682–3695.
[17] M. Dunwell, Q. Lu, J.M. Heyes, J. Rosen, J.G. Chen, Y.S. Yan, F. Jiao, B.J. Xu, J. Am. Chem. Soc. 139 (2017) 3774–3783.
[18] R. Schlogl, Angew. Chem. Int. Ed. 54 (2015) 3465–3520.
[19] W.L. Zhu, Y.J. Zhang, H.Y. Zhang, H.F. Lv, Q. Li, R. Michalsky, A.A. Peterson, S.H. Sun, J. Am. Chem. Soc. 136 (2014) 16132–16135.
[20] D.H. Won, H. Shin, J. Koh, J. Chung, H.S. Lee, H. Kim, S.I. Woo, Angew. Chem. Int. Ed. 55 (2016) 9297–9300.
[21] R.J. Lim, M. Xie, M.A. Alam, J.M. Lee, A. Fisher, X. Wang, K.H. Lim, Catal. Today 233 (2014) 169–180.
[22] R. Kortlever, J. Shen, K.J.P. Schouten, F. Calle–Vallejo, M.T.M. Koper, J. Phys. Chem. Lett. 6 (2015) 4073–4082.
[23] Z.L. Wang, C.L. Li, Y. Yamauchi, Nano Today 11 (2016) 373–391.
[24] A. Demirbas, Energy Combust. Sci. 33 (2007) 1–18.
[25] A.Y. Khodakov, W. Chu, P. Fongarl, Chem. Rev. 107 (2007) 1692–1744.
[26] S. Rasul, D.H. Anjum, A. Jedidi, Y. Minenkov, L. Cavallo, K. Takanabe, Angew. Chem. Int. Ed. 127 (2015) 2174–2178.
[27] K.J.P. Schouten, Z. Qin, E.P. Gallent, M.T.M. Koper, J. Am. Chem. Soc. 134 (2012) 9864–9867.
[28] C.W. Li, J. Ciston, M.W. Kanan, Nature 508 (2014) 504–507.
[29] Y. Hori, in: C. Vayenas, R. White, M.E. Gamboa-Aldeco (Eds.), Mod. Aspects Electrochem., Springer, New York, NY, 2008, pp. 89–189.
[30] W. Zhu, R. Michalsky, O. Metin, H. Lv, S. Guo, C.J. Wright, X. Sun, A.A. Peterson, S. Sun, J. Am. Chem. Soc. 135 (2013) 16833–16836.
[31] Q. Lu, J. Rosen, Y. Zhou, G.S. Hutchings, Y.C. Kimmel, J.G. Chen, F. Jiao, Nat. Commun. 5 (2014) 3242.
[32] Y. Hori, K. Kikuchi, S. Suzuki, Chem. Lett. 11 (1985) 1695–1698.
[33] M. Gattrell, N. Gupta, A. Co, J. Electroanal. Chem. 594 (2006) 1–19.
[34] Y. Hori, A. Murata, R. Takahashi, S. Suzuki, J. Am. Chem. Soc. 109 (1987) 5022–5023.
[35] D.D. Zhu, J.L. Liu, S.Z. Qiao, Adv. Mater. 28 (2016) 3423.
[36] K.P. Kuhl, E.R. Cave, D.N. Abramc, T.F. Jaramillo, Energy Environ. Sci. 5 (2012) 7050–7059.
[37] Y. Hori, A. Murata, R. Takahashi, J. Chem. Soc. Faraday Trans. 85 (1989) 2309–2326.
[38] Y. Hori, I. Takahashi, O. Koga, N. Hoshi, J. Phys. Chem. B 106 (2002) 15–17.
[39] N. Gupta, M. Gattrell, B. MacDougall, J. Appl. Electrochem. 36 (2006) 161–172.
[40] K.J.P. Schouten, Y. Kwon, C.J.M. van der Ham, Z. Qin, M.T.M. Koper, Chem. Sci. 2 (2011) 1902–1909.
[41] J.J. Bei, R. Zhang, Z.D. Chen, W.X. Lv, W. Wang, Int. J. Electrochem. Sci. 12 (2017) 2365–2375.
[42] Y. Zhao, C.Y. Wang, G.G. Wallace, J. Mater. Chem. A 4 (2016) 10710–10718.
[43] A. Lavacchi, H. Miller, F. Vizza, Nanotechnology in Electrocatalysis for Energy, Springer, New York, NY, 2013, pp. 25–61.
[44] J.T. Zhang, H.L. Li, P.Z. Guo, H.Y. Ma, X.S. Zhao, J. Mater. Chem. A 4 (2016) 8497–8511.
[45] Y.H. Chen, M.W. Kanan, J. Am. Chem. Soc. 134 (2012) 1986–1989.
[46] Y. Chen, C.W. Li, M.W. Kanan, J. Am. Chem. Soc. 134 (2012) 19969–19972.
[47] S. Trasatti, O.A. Petrii, Pure Appl. Chem. 65 (1991) 711–734.
[48] G.Y. Wu, S.E. Bae, A.A. Gewirth, J. Gray, X.D. Zhu, T.P. Moffat, W. Schwarzacher, Surf. Sci. 601 (2007) 1886–1891.
[49] D. Raciti, K.J. Livi, C. Wang, Nano Lett. 15 (2015) 6829–6835.
[50] Y. Song, R. Peng, D.K. Hensley, P.V. Bonnesen, L.B. Liang, Z.L. Wu, H.M. Meyer, M.F. Chi, C. Ma, B.G. Sumpter, A.J. Rondinone, ChemistrySelect 1 (2016) 1–8.
[51] T.T.H. Hoang, S.C. Ma, J.I. Gold, P.J.A. Kenis, A.A. Gewirth, ACS Catal. 7 (2017) 3313–3321.
[52] Y. Yoon, A.S. Hall, Y. Surendranath, Angew. Chem. Int. Ed. 55 (2016) 15282–15286.

[53] S.C. Ma, M. Sadakiyo, M. Heima, R. Luo, R.T. Haasch, J.I. Gold, M. Yamauchi, P.J.A. Kenis, J. Am. Chem. Soc. 139 (2017) 47–50.
[54] M. Asadi, K. Kim, C. Liu, A.V. Addepalli, P. Abbasi, P. Yasaei, P. Phillips, A. Behranginia, J.M. Cerrato, R. Haasch, P. Zapol, B. Kumar, R.F. Klie, J. Abiade, L.A. Curtiss, A. Salehi–Khojin, Science 253 (2016) 467–470.
[55] J. Kibsgaard, C. Tsai, K. Chan, J.D. Benck, J.K. Nørskov, F. Abild–Pedersen, T.F. Jaramillo, Energy Environ. Sci. 8 (2015) 3022–3029.
[56] B. An, J.Z. Zhang, K. Cheng, P.F. Ji, C. Wang, W.B. Lin, J. Am. Chem. Soc. 139 (2017) 3834–3840.
[57] R. Reske, H. Mistry, F. Behafarid, B.R. Cuenya, P. Strasser, J. Am. Chem. Soc. 136 (2014) 6978–6986.
[58] W.J. Durand, A.A. Peterson, F. Abild–Pedersen, J.K. Norskov, Surf. Sci. 605 (2011) 1354–1359.
[59] J. Medina–Ramos, J.L. DiMeglio, J. Rosenthal, J. Am. Chem. Soc. 13 (2014) 8361–8367.
[60] R. Kas, K.K. Hummadi, R. Kortlever, P. Wit, A. Milbrat, M.W.J. Luiten–Olieman, N.E. Benes, M.T.M. Koper, G. Mul, Nat. Commun. 7 (2016) 10748.
[61] Y. Gendel, H. Roth, A. Rommerskirchen, O. David, M. Wessling, Electrochem. Commun. 4 (2014) 44–47.
[62] Y. Chen, C.W. Li, M.W. Kanan, J. Am. Chem. Soc. 13 (2012) 19969–19972.
[63] S. Sen, D. Liu, G.T.R. Palmore, ACS Catal. 4 (2014) 3091–3095.
[64] A. Dutta, M. Rahaman, N.C. Luedi, M. Mohos, P. Broekmann, ACS Catal. 6 (2016) 3804–3814.
[65] H.C. Shin, J. Dong, M.L. Liu, Adv. Mater. 15 (2003) 1640.
[66] H.C. shin, M.L. Liu, Chem. Mater. 16 (2004) 5460–5464.
[67] F.S. Roberts, K.P. Kuhl, A. Nilsson, Angew. Chem. Int. Ed. 127 (2015) 5268–5271.
[68] H. Chen, M. Zhou, T. Wang, F. Lia, Y.X. Zhang, J. Mater. Chem. A 4 (2016) 10786–10793.
[69] H. Chen, X.Q. Qi, M. Kuang, F. Dong, Y.X. Zhang, Electrochim. Acta 212 (2016) 671–677.
[70] M. Huang, Y.X. Zhang, F. Li, Z.C. Wang, Alamusi, N. Hu, Z.Y. Wen, Q. Liu, Sci. Rep. 4 (2014) 4518.
[71] A.A. Peterson, F. Abild–Pedersen, F. Studt, J. Rossmeisl, J.K. Norskov, Energy Environ. Sci. 3 (2010) 1311–1315.
[72] Z. Yin, D.F. Gao, S.Y. Yao, B. Zhao, F. Cai, L.L. Lin, P. Tang, P. Zhai, G.X. Wang, D. Ma, X.H. Bao, Nano Energy 27 (2016) 35–43.
[73] Q. Li, J.Y. Fu, W.L. Zhu, Z.Z. Chen, B. Shen, L.H. Wu, Z. Xi, T.Y. Wang, G. Lu, J.J. Zhu, S.H. Sun, J. Am. Chem. Soc. 139 (2017) 4290–4293.
[74] K. Larmier, W.C. Liao, S. Tada, E. Lam, R. Verel, A. Bansode, A. Urakawa, A. Comas-Vives, C. Coperet, Angew. Chem. Int. Ed. 56 (2017) 2318–2323.
[75] S. Kattel, P.J. Ramírez, J.G. Chen, J.A. Rodriguez, P. Liu, Science 355 (2017) 1296–1299.
[76] S. Ma, M. Sadakiyo, R. Luo, M. Heima, P. Yamauchi, J.A. Kenis, J. Power Sources 301 (2016) 219–228.
[77] A.A. Peterson, J.K. Nørskov, J. Phys. Chem. Lett. 3 (2012) 251–258.
[78] S.X. Bai, Q. Shao, P.T. Wang, Q.G. Dai, X.Y. Wang, X.Q. Huang, J. Am. Chem. Soc. 139 (2017) 6827–6830.
[79] G.O. Larrazábal, A.J. Martín, S. Mitchell, R. Hauert, J.P. Ramírez, ACS Catal. 6 (2016) 6265–6274.
[80] A. Jedidi, S. Rasul, D. Masih, L. Cavallo, K. Takanabe, J. Mater. Chem. A 3 (2015) 19085–19092.
[81] T.F Li, C.P. Berlinguette, Angew. Chem. Int. Ed. 56 (2017) 6068–6072.
[82] Z.M. Detweiler, J.L. White, S.L. Bernasek, A.B. Bocarsly, Langmuir 30 (2014) 7593–7600.
[83] J. Guo, S. Ouyang, T. Kako, J. Ye, Appl. Surf. Sci. 280 (2013) 418–423.
[84] S. Kapusta, N. Hackerman, J. Electrochem. Soc. 130 (1983) 607–613.
[85] M. Liu, Y. Pang, B. Zhang, D.P. Luna, O. Voznyy, J. Xu, X. Zheng, C.T. Dinh, F. Fan, C. Cao, F.P.G. Arquer, T.S. Safaei, A. Mepham, A. Klinkova, E. Kumacheva, T. Filleter, D. Sinton, S.O. Kelley, E.H. Sargent, Nature 537 (2016) 382–386.
[86] Y. Li, W. Gao, L. Ci, C. Wang, P. Ajayan, Carbon 48 (2010) 1124–1130.
[87] G. Jeong, S. Suzuki, Y. Kobayashi, Nanotechnology 20 (2009) 285708-258713.
[88] W. Lee, U. Maiti, J. Lee, J. Lim, T. Han, S. Kim, Chem. Commun. 50 (2014) 6818–6830.
[89] C. Kim, H.S. Jeon, T. Eom, M.S. Jee, H. Kim, C.M. Friend, B.K. Min, Y.J. Hwang, J. Am. Chem. Soc. 137 (2015) 13844–13850.
[90] M. Ding, Y. Tang, A.J. Star, Phys. Chem. Lett. 4 (2013) 147–160.
[91] S. Navalon, A. Dhakshinamoorthy, M. Alvaro, H.C. Garcia, Chem. Rev. 312 (2016) 99–148.
[92] M. Liu, R. Zhang, W. Chen, Chem. Rev. 114 (2014) 5117–5160.
[93] J. Saavedra, H.A. Doan, C.J. Pursell, L.C. Grabow, B.D. Chandler, Science 345 (2014) 1599–1602.
[94] J.Y. Park, L.R. Baker, G.A. Somorjai, Chem. Rev. 115 (2015) 2781–2817.
[95] J. Graciani, K. Mudiyanselage, F. Xu, A.E. Baber, J. Evans, S.D. Senanayake, D.J. Stacchiola, P. Liu, J. Hrbek, J.F. Sanz, J.A. Rodriguez, Science 345 (2014) 546–550.
[96] D. Wang, Q. Bi, G. Yin, W. Zhao, F. Huang, X. Xie, M. Jiang, Chem. Commun. 52 (2016) 14226–14229.
[97] C. Rogers, W.S. Perkins, G. Veber, T.E. Williams, R.R. Cloke, F.R. Fischer, J. Am. Chem. Soc. 139 (2017) 4052–4061.
[98] D.T. Whipple, P.J.A. Kenis, J. Phys. Chem. Lett. 1 (2010) 3451–3458.
[99] M. Watanabe, M. Shibata, A. Kato, M. Azuma, T.J. Sakata, J. Electrochem. Soc. 138 (1991) 3382–3389.
[100] Q. Li, W.L. Zhu, J.J. Fu, H.Y. Zhang, G. Wu, S.H. Sun, Nano Energy 24 (2016) 1–9.
[101] I. Hod, M.D. Sampson, P. Deria, C.P. Kubiak, O.K. Farha, J.T. Hupp, ACS Catal. 5 (2015) 6302–6309.
[102] N. Kornienko, Y. Zhao, C.S. Kley, C. Zhu, D. Kim, S. Lin, C.J. Chang, O.M. Yaghi, P. Yang, J. Am. Chem. Soc. 137 (2015) 14129–14135.
[103] J. Albo, D. Vallejo, G. Beobide, O. Castillo, P. CastaÇo, A. Irabien, ChemSusChem 9 (2016) 1–11.
[104] R.S. Kumar, S.S. Kumar, M.A. Kulandainathan, Electrochem. Commun. 25 (2012) 70–73.
[105] T. Maihom, S. Wannakao, B. Boekfa, J. Limtrakul, J. Phys. Chem. C. 117 (2013) 17650–17658.
[106] H. Hu, L. Han, M. Yu, Z. Wang, X.W. Lou, Energy Environ. Sci. 9 (2016) 107–111.
[107] L. Yang, M. Gao, B. Dai, X. Guo, Z. Liu, B. Peng, Electrochim. Acta 191 (2016) 813–820.
[108] K. Zhao, Y.M. Liu, X. Quan, S. Chen, H.T. Yu, ACS Appl. Mater. Interfaces 9 (2017) 5302–5311.
[109] M. Le, M. Ren, Z. Zhang, P.T. Sprunger, R.L. Kurtz, J.C. Flake, J. Electrochem. Soc. 158 (2011) E45–E49.
[110] K.W. Frese, J. Electrochem. Soc. 138 (1991) 3338–3344.
[111] Y. Gao, F. Wu, H. Chen, J. Energy Chem. 26 (2017) 428–432.
[112] V.M. Bau, X.J. Bo, L.P. Guo, J. Energy Chem. 26 (2017) 63–71.